(Version of March 11, 2009)

A MATHEMATICAL MODEL COMPARING SOLUTE KINETICS IN LOW- AND HIGH-BMI HEMODIALYSIS PATIENTS

F. KAPPEL[1], J. J. BATZEL [1], M. BACHAR [2], AND P.KOTANKO [3]

[1]Institute for Mathematics and Scientific Computing, University of Graz
[2] Department of Mathematics, King Saud University, Saudi Arabia
[3] Renal Research Institute, New York

Abstract. Dialysis patients with high body mass index (BMI) experience survival advantages as compared to patients with smaller BMI. This study aimed to model uremic toxin concentrations in patients exhibiting a wide range in BMI. The first aim was to examine how BMI contributed to heightened or reduced levels of toxin and to test whether the model provided support for the hypothesis that the observed enhanced survivability rates for patients with higher versus lower BMI might be related to a differential in toxin levels. A second aim was to carry out a classical and generalized sensitivity analysis to examine what types of data and experiments might allow for model validation.

1. Introduction

Dialysis patients with high body mass index (BMI) experience survival advantages as compared to patients with smaller BMI. Research related to this phenomenon can be found in [9], [10], [2], and [5].

Body mass index is defined as the ratio of an individual's height to the square of the individual's weight (unit kg/m^2). Developed over a hundred years ago, it is an indicator of the deviation of an individual's weight from what would be considered normal (and healthy). The World Health Organization has given the following ranges. Underweight is given to be in the range from 16 to 18.5, Normal from 18.5 to 25.0, Overweight from 25.0 to 30.0, and Obese class I from 30.0 to 35. BMI ranges can vary with nationality and age. This index represents information on the relation of weight to health risks, with higher than normal BMI raising the risk for cardiovascular and other diseases.

It is odd then that there is reported increased survival advantage for dialysis patients with high BMI. A number of hypotheses have been put forward to explain this anomaly. See for example [3] and [5].

The kidney is the primary organ for removing toxic byproducts and wastes of metabolism and also for the regulation of body fluid content. When the kidney fails, uremic toxins and body fluid accumulate requiring dialysis which is a medical intervention for removing these accumulated toxins, wastes, and excess body fluid.

One hypothesis for the survival advantage of larger BMI dialysis patients involves the fact that, in terms of body size as measured by BMI, the proportion of organs that produce uremic toxins to total body size, is larger in subjects with lower body mass. Thus, as BMI increases, the ratio of toxin producing organs to total body

Key words and phrases.

size decreases. This implies higher concentration of extracellular uremic toxins in lower BMI dialysis patients. These toxins can damage tissue.

A second and related hypothesis is that body muscle tissue and adipose (fat) tissue absorb and release toxins from the blood acting as buffers to extracellular levels of toxins. During dialysis (the intra-dialytic phase), all of the uremic toxins are quickly removed from the extracellular space. Between dialysis treatments (inter-dialytic phase) toxins which were accumulated in muscle and fat tissue are gradually returned to the extracellular fluid. Depending on the buffering (determined by compartment exchange rates), it might be the case that adipose tissue acts as a better buffer, returning toxins between dialysis treatments more slowly, and hence helping to restrict the concentration of toxins in the extracellular space. Hence high BMI patients would have a lower average concentration of uremic toxins, and reduced damage from these toxins.

This paper examines these hypotheses which were outlined in [3]. Other explanations and mechanisms are also possible as can be seen in [5].

2. The model

The model is a compartment model with the following four compartments:

- the extracellular fluid compartment E,
- the organ mass compartment OM,
- the muscle tissue compartment MT,
- the adipose tissue compartment AT,
- the storage compartment S in case of the extended model.

These compartments are characterized by their volumes, V_{E}, V_{OM}, V_{MT}, V_{AT}, and the mass of toxin contained in the compartment, x_{E}, x_{OM}, x_{MT}, x_{AT}. The concentration of the toxin in these compartments is denoted by C_{E}, C_{OM}, C_{MT} and C_{AT}. Of course, we have

$$C_{\mathsf{E}} = \frac{x_{\mathsf{E}}}{V_{\mathsf{E}}}, \quad C_{\mathsf{OM}} = \frac{x_{\mathsf{OM}}}{V_{\mathsf{OM}}}, \quad C_{\mathsf{MT}} = \frac{x_{\mathsf{MT}}}{V_{\mathsf{MT}}}, \quad C_{\mathsf{AT}} = \frac{x_{\mathsf{AT}}}{V_{\mathsf{AT}}}.$$

The model for the dynamics of the toxin mass in each compartment of the system will be developed under the following assumptions:

(A1) Exchange of toxin is only between compartment E and the compartments OM, MT, AT. In case of the extended model the exchange of toxin in the compartment S is only with compartment AT.

(A2) The exchange of toxins between compartments is mainly due to diffusion processes.

According to assumption (A2) the flux q of toxin from compartment I into compartment II is given by

$$q = k_{\mathsf{I},\mathsf{II}}\big(C_{\mathsf{I}} - C_{\mathsf{II}}\big),$$

where C_{I}, C_{II} are the concentrations of toxin in the two compartments and $k_{\mathsf{I},\mathsf{II}}$ is a positive constant, the diffusion of toxin from compartment I into compartment II. If q is negative then the flux is from compartment II into compartment I, of course. The masses x_{I}, x_{II} of toxin in the two compartments will change in time according

to the following equations:

$$\dot{x}_{\mathsf{I}} = -k_{\mathsf{I},\mathsf{II}}\big(C_{\mathsf{I}} - C_{\mathsf{II}}\big) = -\frac{k_{\mathsf{I},\mathsf{II}}}{V_{\mathsf{I}}}x_{\mathsf{I}} + \frac{k_{\mathsf{I},\mathsf{II}}}{V_{\mathsf{II}}}x_{\mathsf{II}},$$
$$\dot{x}_{\mathsf{II}} = k_{\mathsf{I},\mathsf{II}}\big(C_{\mathsf{I}} - C_{\mathsf{II}}\big) = \frac{k_{\mathsf{I},\mathsf{II}}}{V_{\mathsf{I}}}x_{\mathsf{I}} - \frac{k_{\mathsf{I},\mathsf{II}}}{V_{\mathsf{II}}}x_{\mathsf{II}},$$

where V_{I}, V_{II} are the volumes of compartments I and II.

We have to consider the diffusion constants $k_{\mathsf{E},\mathsf{OM}}$, $k_{\mathsf{E},\mathsf{MT}}$ and $k_{\mathsf{E},\mathsf{AT}}$. Furthermore, we denote by G the production rate of the toxin in compartment OM. During dialysis we have a clearance rate k_{clear} of the toxin from the compartment E. Next we derive differential equations for the dynamics of the toxin mass in each compartment.

a) The compartment OM.
According to our considerations from above we get

$$\dot{x}_{\mathsf{OM}} = G - \frac{k_{\mathsf{E},\mathsf{OM}}}{V_{\mathsf{OM}}}x_{\mathsf{OM}} + \frac{k_{\mathsf{E},\mathsf{OM}}}{V_{\mathsf{E}}}x_{\mathsf{E}}. \tag{1}$$

b) The compartment MT.
We have

$$\dot{x}_{\mathsf{MT}} = \frac{k_{\mathsf{E},\mathsf{MT}}}{V_{\mathsf{E}}}x_{\mathsf{E}} - \frac{k_{\mathsf{E},\mathsf{MT}}}{V_{\mathsf{MT}}}x_{\mathsf{MT}}. \tag{2}$$

c) The compartment AT.
The equation for this compartment is analogous to the one for the compartment MT:

$$\dot{x}_{\mathsf{AT}} = \frac{k_{\mathsf{E},\mathsf{AT}}}{V_{\mathsf{E}}}x_{\mathsf{E}} - \frac{k_{\mathsf{E},\mathsf{AT}}}{V_{\mathsf{AT}}}x_{\mathsf{AT}}. \tag{3}$$

d) The compartment E.
The source term for this compartment is the sum of loss terms of the other compartments, whereas the loss term is the sum of the source terms of the other compartments plus a term describing the clearance of the toxin during dialysis:

$$\begin{aligned}\dot{x}_{\mathsf{E}} = {} & \frac{k_{\mathsf{E},\mathsf{OM}}}{V_{\mathsf{OM}}}x_{\mathsf{OM}} + \frac{k_{\mathsf{E},\mathsf{MT}}}{V_{\mathsf{MT}}}x_{\mathsf{MT}} + \frac{k_{\mathsf{E},\mathsf{AT}}}{V_{\mathsf{AT}}}x_{\mathsf{AT}} \\ & - \frac{1}{V_{\mathsf{E}}}\big(k_{\mathsf{E},\mathsf{OM}} + k_{\mathsf{E},\mathsf{MT}} + k_{\mathsf{E},\mathsf{AT}}\big)x_{\mathsf{E}} - K_{\text{clearance}},\end{aligned} \tag{4}$$

where

$$K_{\text{clearance}} = \begin{cases} k_{\text{clear}}x_{\mathsf{E}} & \text{during dialysis,} \\ 0 & \text{during the interdialytic phase.} \end{cases}$$

Equations (1) – (4) can be written as a linear system of ordinary differential equations:

$$\frac{d}{dt}\begin{pmatrix} x_{\mathsf{OM}} \\ x_{\mathsf{MT}} \\ x_{\mathsf{AT}} \\ x_{\mathsf{E}} \end{pmatrix} = AV\begin{pmatrix} x_{\mathsf{OM}} \\ x_{\mathsf{MT}} \\ x_{\mathsf{AT}} \\ x_{\mathsf{E}} \end{pmatrix} + \begin{pmatrix} G \\ 0 \\ 0 \\ 0 \end{pmatrix}, \tag{5}$$

where

$$A = \begin{pmatrix} -k_{\mathsf{E,OM}} & 0 & 0 & k_{\mathsf{E,OM}} \\ 0 & -k_{\mathsf{E,MT}} & 0 & k_{\mathsf{E,MT}} \\ 0 & 0 & -k_{\mathsf{E,AT}} & k_{\mathsf{E,AT}} \\ k_{\mathsf{E,OM}} & k_{\mathsf{E,MT}} & k_{\mathsf{E,AT}} & -(k_{\mathsf{E,OM}} + k_{\mathsf{E,MT}} + k_{\mathsf{E,AT}} + \delta k_{\mathrm{clear}}) \end{pmatrix},$$

$$V = \mathrm{diag}\Big(\frac{1}{V_{\mathsf{OM}}}, \frac{1}{V_{\mathsf{MT}}}, \frac{1}{V_{\mathsf{AT}}}, \frac{1}{V_{\mathsf{E}}}\Big)$$

and $\delta = 1$ during dialysis (and 0 otherwise).

Of course, we also can write the equations in terms of the concentrations:

$$\frac{d}{dt}\begin{pmatrix} C_{\mathsf{OM}} \\ C_{\mathsf{MT}} \\ C_{\mathsf{AT}} \\ C_{\mathsf{E}} \end{pmatrix} = VA \begin{pmatrix} C_{\mathsf{OM}} \\ C_{\mathsf{MT}} \\ C_{\mathsf{AT}} \\ C_{\mathsf{E}} \end{pmatrix} + \begin{pmatrix} G/V_{\mathsf{OM}} \\ 0 \\ 0 \\ 0 \end{pmatrix}, \tag{6}$$

where we have used that $\mathrm{col}(C_{\mathsf{OM}}, C_{\mathsf{MT}}, C_{\mathsf{AT}}, C_{\mathsf{E}}) = V\,\mathrm{col}(x_{\mathsf{OM}}, x_{\mathsf{MT}}, x_{\mathsf{AT}}, x_{\mathsf{E}})$.

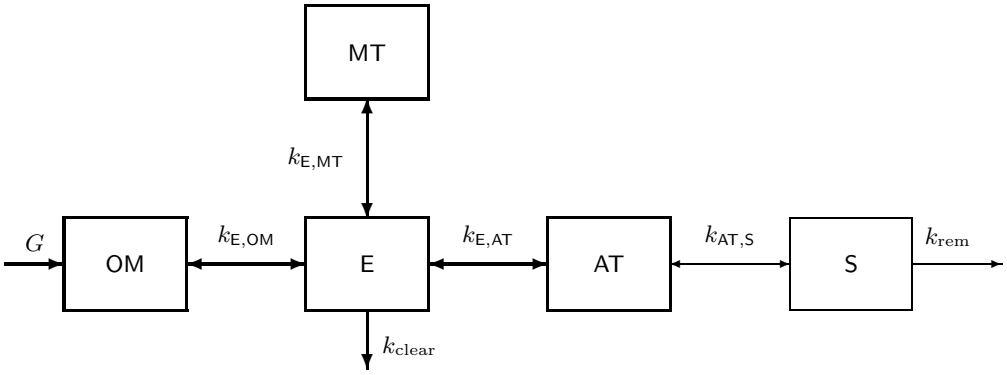

Figure 1: Structure of the model (extensions in thin lines).

As a modification of the basic model we assume that the adipose tissue compartment AT is connected to a storage compartment S for the toxin. Also here we assume that transport of the toxin between the compartments S and AT is primarily by diffusion. However, we also assume that there is a saturation level $c_{\max}$ for the toxin in compartment S, i.e., if the concentration C_{S} of toxin in compartment S is greater or equal $c_{\max}$, then no transport of toxin from compartment AT into compartment S is possible. This is achieved by setting the diffusion constant $k_{\mathsf{AT,S}}$, which governs diffusion of the toxin between compartments AT and S, to zero if $C_{\mathsf{S}} \geq c_{\max}$. Furthermore, we assume that the rate constant for the transport of toxin from the compartment AT to the storage compartment S is by a factor $\gamma > 1$ larger than the rate constant for the transport of toxin from compartment S into compartment AT. Thus we have

$$k_{\mathsf{AT,S}} = \begin{cases} 0 & \text{for } C_{\mathsf{AT}} \geq C_{\mathsf{S}} > c_{\max}, \\ k^{(0)}_{\mathsf{AT,S}} & \text{for } C_{\mathsf{AT}} < C_{\mathsf{S}}, \\ \gamma k^{(0)}_{\mathsf{AT,S}} & \text{for } C_{\mathsf{S}} \leq \min(C_{\mathsf{AT}}, c_{\max}), \end{cases}$$

where $k^{(0)}_{\mathsf{AT,S}} > 0$ is given.

The differential equations for compartments AT and S now are given by

$$\dot{C}_{\mathsf{AT}} = -\frac{k_{\mathsf{E,AT}} + k_{\mathsf{AT,S}}}{V_{\mathsf{AT}}} C_{\mathsf{AT}} + \frac{k_{\mathsf{E,MT}}}{V_{\mathsf{AT}}} C_{\mathsf{E}} + \frac{k_{\mathsf{AT,S}}}{V_{\mathsf{AT}}} C_{\mathsf{S}},$$
$$\dot{C}_{\mathsf{S}} = \frac{k_{\mathsf{AT,S}}}{V_{\mathsf{S}}} C_{\mathsf{AT}} - \frac{k_{\mathsf{AT,S}}}{V_{\mathsf{S}}} C_{\mathsf{S}}.$$

In addition, we also consider degradation of the toxin in the storage compartment S at a rate k_{rem}. In this case the equation governing the toxin concentration in compartment S is

$$\dot{C}_{\mathsf{S}} = \frac{k_{\mathsf{AT,S}}}{V_{\mathsf{S}}} C_{\mathsf{AT}} - \frac{k_{\mathsf{AT,S}} + k_{\mathrm{rem}}}{V_{\mathsf{S}}} C_{\mathsf{S}}.$$

3. Parameters

In [3] three patient classes, each one represented by a 'typical' patient are considered. The typical large, medium respectively small patient has weight 100 kg, 70 kg respectively 40 kg and size $h = 1.6$ m. From these assumptions the volumes (in liters) of the compartments of the model are determined in [3] as follows:

a) *The organ mass compartment* OM.
A linear regression gives the percentage of body weight (BW) by the organ mass:

$$\frac{\mathsf{OM}_{\mathrm{weight}}}{\mathsf{BW}} \approx 0.33 - 0.0012\,\mathsf{BW}. \tag{7}$$

Multiplying by BW and taking into account, that the average density of the human body is ~ 1 kg/L, we obtain

$$V_{\mathsf{OM}} = \mathsf{BW}(0.33 - 0.0012\,\mathsf{BW}). \tag{8}$$

b) *The toxin production rate* G.
In order to obtain the toxin production rate G we start with a linear regression:

$$G \approx 4.2\,\mathsf{OM}_{\mathrm{weight}} - 4,$$

which provides G in units of mass per day. Using (7) we get

$$G \approx \mathsf{BW}(1.4 - 0.005\,\mathsf{BW}) - 4. \tag{9}$$

In our simulations we used a constant rate of 0.15 units of mass per minute.

c) *The extracellular fluid compartment* E.
The volume of the extracellular fluid compartment is the total body water (TBW) minus the intracellular fluid volume (IFV). We have $\mathsf{TBW} \approx 0.58\,\mathsf{BW}$ and $\mathsf{IFV} \approx 0.2\mathsf{BW}$, i.e.,

$$V_{\mathsf{E}} \approx \mathsf{TBW} - \mathsf{IFV} = 0.38\,\mathsf{BW}. \tag{10}$$

In [3] the term IFV is neglected. In our simulations we used the value given by $0.58\,\mathsf{BW}$ as in [3].

d) *The muscle tissue compartment* MT.
In order to obtain the total muscle tissue volume $V_{\mathsf{MT,total}}$ we start with the linear regression

$$V_{\mathsf{MT,total}} \approx 0.76\,\mathsf{TBW} - 6.8.$$

Using $\mathsf{TBW} \approx 0.58\mathsf{BW}$ we get

$$V_{\mathsf{MT},\text{total}} \approx 0.44\,\mathsf{BW} - 6.8 \text{ liters.}$$

The effective muscle tissue volume V_{MT} is given by

$$V_{\mathsf{MT}} \approx 0.75\,V_{\mathsf{MT},\text{total}} \approx 0.33\,\mathsf{BW} - 5.1 \text{ liters.} \tag{11}$$

This formula obviously is not used in [3]. For $\mathsf{BW} = 100$ kg, for instance, we get $V_{\mathsf{MT}} \approx 27.9$ L. On the other hand, Table II of [3] shows $V_{\mathsf{MT}} + V_{\mathsf{AT}} = 11$ L in this case. In our simulations we use the values for V_{MT} as given in [3].

e) *The adipose tissue compartment* AT.
Concerning the adipose tissue volume we start with the linear regression

$$V_{\mathsf{AT},\text{total}} \approx 1.89\,\mathsf{BMI} - 29.2 = \begin{cases} 44.62 & \text{for the “large” person,} \\ 22.47 & \text{for the “medium” person,} \\ 0.34 & \text{for the “small” person.} \end{cases}$$

The effective adipose tissue volume V_{AT} is given by

$$V_{\mathsf{AT}} \approx 0.1\,V_{\mathsf{AT},\text{total}} \approx 0.189\,\mathsf{BMI} - 2.92 \approx 0.189\frac{\mathsf{BW}}{h^2} - 2.92 \text{ liters.} \tag{12}$$

For the extended model we also need V_{S}, which is given by

$$V_{\mathsf{S}} = 0.9\,V_{\mathsf{AT},\text{total}},$$

i.e.,

$$V_{\mathsf{S}} = \begin{cases} 40.16 & \text{for the “large” person,} \\ 20.23 & \text{for the “medium” person,} \\ 0.31 & \text{for the “small” person.} \end{cases}$$

In [3] The muscle tissue and the adipose tissue compartments are lumped together to one compartment MAT with

$$V_{\mathsf{MAT}} = V_{\mathsf{MT}} + V_{\mathsf{AT}} \text{ liters.}$$

Adding up the formulas for V_{OM}, V_{MT}, V_{AT} and V_{E} as given in [3] we obtain

$$V_{\text{total}} = 1.113\,\mathsf{BW} - 8.02 - 0.0012\,\mathsf{BW}^2,$$

which implies

$$V_{\text{total}} = \begin{cases} 91.28 & \text{if } \mathsf{BW} = 100, \\ 64.01 & \text{if } \mathsf{BW} = 70, \\ 34.58 & \text{if } \mathsf{BW} = 40 \end{cases}$$

in discrepancy with the values given in [3] for the total volumes (see the entries for V_{total} in Table 1).

For our simulations we took the volumes as given in Table 1, the rate constants given in Table 2 and the initial values for the concentrations given in Table 3.

For all simulations of the extended model we used $c_{\max} = 10$ and $\gamma = 5$.

4. Some simulations

In this section we present some of the simulation with the model developed in Section 1 using the volumes given in Table 1 and the rate constants given in Table 2.

size	V_{E}	V_{OM}	V_{MT}	V_{AT}	V_{MAT}	V_{total}	BW	BMI
large	58	21	6.54	4.46	11	90	100	39.06
medium	40.6	17.22	2.93	2.25	5.18	63	70	27.34
small	23.2	11.28	1.486	0.034	1.52	36	40	15.63

size	$V_{\mathsf{E}}/V_{\text{total}}$	$V_{\mathsf{OM}}/V_{\text{total}}$	$V_{\mathsf{MT}}/V_{\text{total}}$	$V_{\mathsf{AT}}/V_{\text{total}}$	sum	G
large	0.6444	0.2333	0.0727	0.0496	1	0.3
medium	0.6444	0.2733	0.0465	0.0357	1	0.3
small	0.6444	0.3133	0.0413	0.0009	1	0.3

Table 1: Parameters used for the simulations. Upper part: Volumes (in liters), bodyweight (in kg) and body mass index (in kg/m^2) for a typical large, medium and small person. Lower part: Percentage of volumes and toxin production rate G for a typical large, medium and small person.

$k_{\mathsf{E,OM}}$	$k_{\mathsf{E,MT}}$	$k_{\mathsf{E,AT}}$	k_{clear}
0.045	0.03177	0.0193	0.1

Table 2: Rate constants used for all simulations.

C_{OM}	C_{MT}	C_{AT}	C_{E}	C_{S}
35	35	35	35	20

Table 3: Initial values for the simulations.

4.1. Simulations for the basic model. In Figures 2 we present the simulations for the typical large, the typical medium and the typical small person over 3 cycles (one cycle is the interdialytic phase plus the dialysis phase) for the basic model given by (6). The graphs show the time behavior of the toxin concentration in the compartments OM, MT, AT, E. We see that the solutions of the model approach a periodic solution as time increases. In Figure 3 the toxin concentrations during one cycle of this periodic solution are shown. In Figure 4 we present the toxin concentration in the extracellular compartment during one cycle. We clearly can see that the concentration for the large person is lowest during the cycle, whereas the concentration for the small person is largest during a major part of the cycle. This is also reflected by the values for the average toxin concentration during the interdialytic period as given in Table 4.

Person	large	medium	small
TAC	36.86	43.75	48.36

Table 4: Average concentration of the toxin during the interdialytic phase in case of the basic model ($k^{(0)}_{\mathsf{AT,S}} = 0$, $k_{\mathsf{rem}} = 0$).

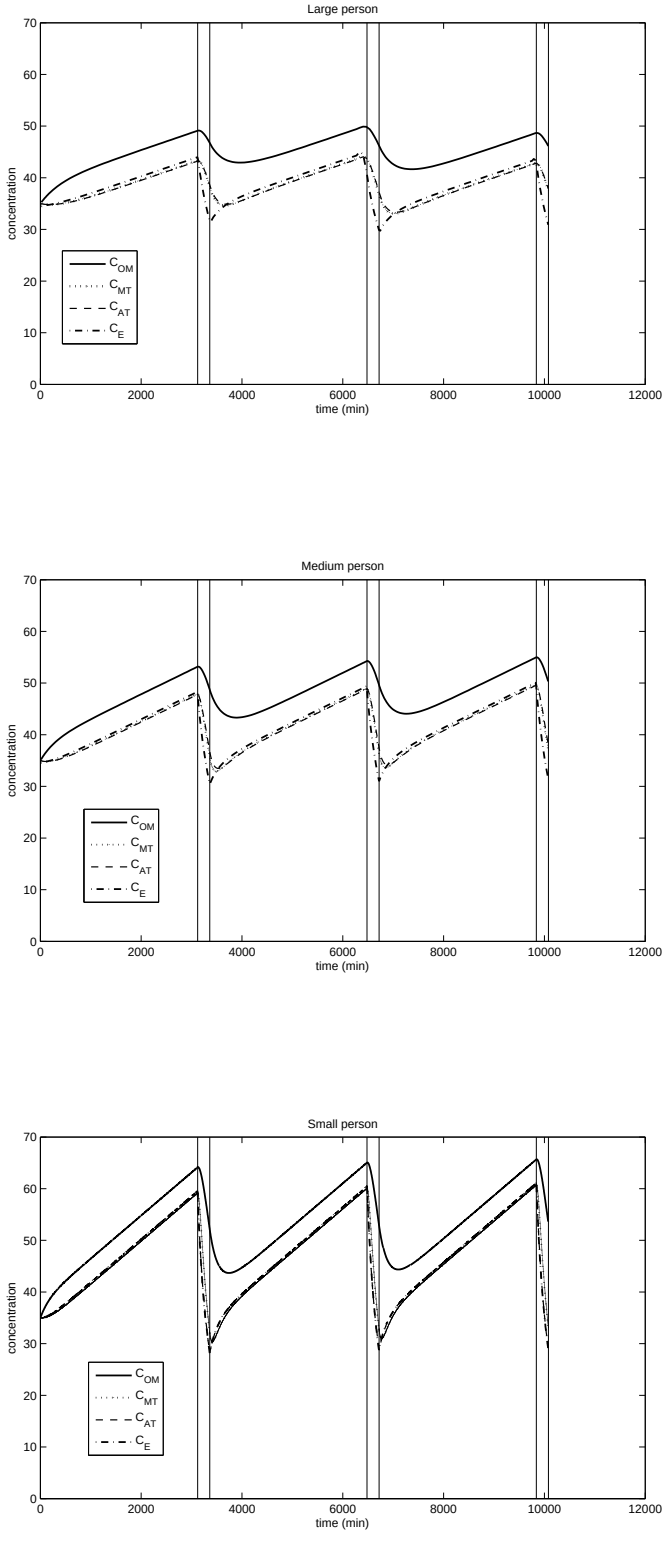

Figure 2: Simulation over three cycles for the time behavior of the toxin concentration in the compartments of the basic model ($k^{(0)}_{\mathsf{AT,S}} = 0$, $k_{\mathsf{rem}} = 0$).

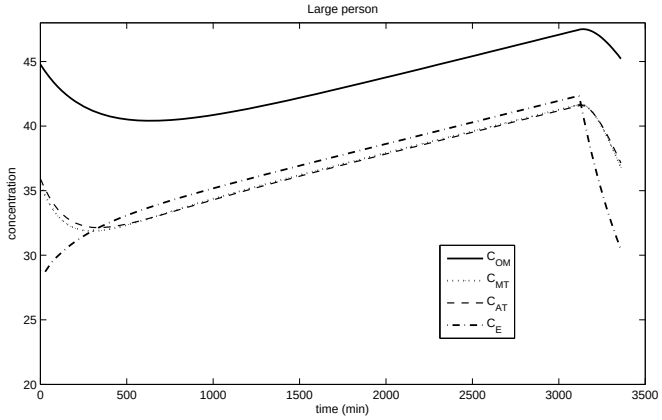

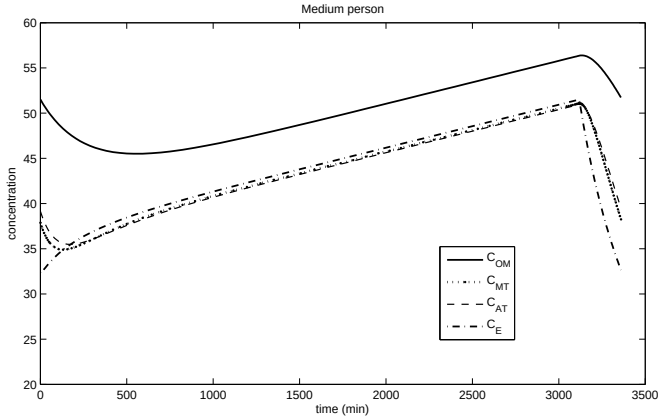

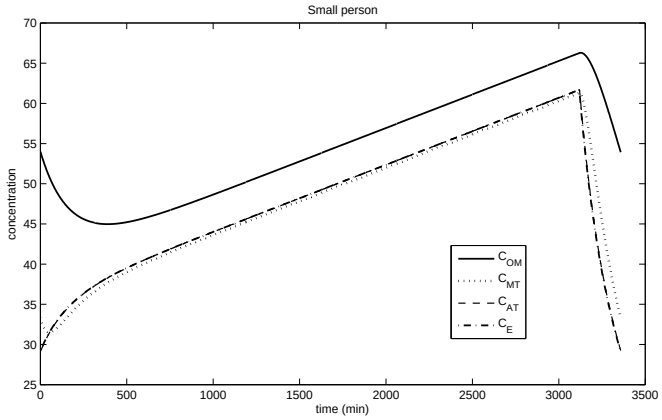

Figure 3: Simulation for the time behavior during the interdialytic period of the toxin concentration in the compartments of the basic model ($k^{(0)}_{\mathsf{AT,S}} = 0,\ k_{\mathsf{rem}} = 0$).

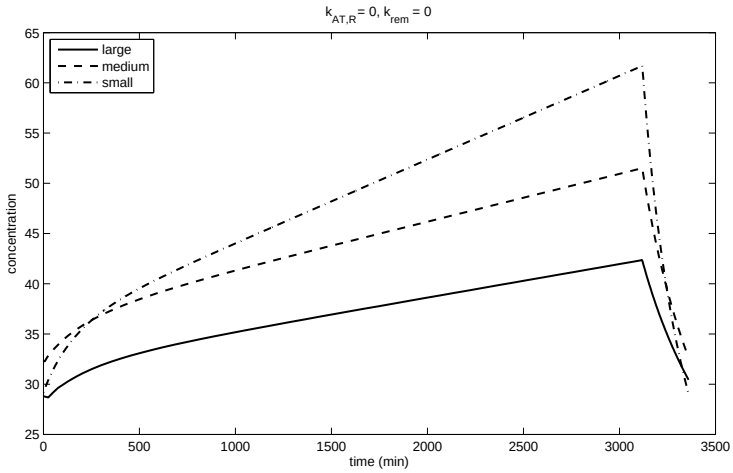

Figure 4: Comparison of the toxin concentration in the extracellular compartment for the basic model ($k^{(0)}_{\mathsf{AT,S}} = 0$, $k_{\mathsf{rem}} = 0$).

4.2. Simulations for the model with storage compartment. In Figure 5 we present the simulations for the large, medium sized and small person over three cycles in case of the model with storage compartment, however without degradation of the toxin in this compartment, i.e., we have $k^{(0)}_{\mathsf{AT,S}} = 0.05$ and $k_{\mathrm{rem}} = 0$. Figure 6 presents the corresponding simulations over one cycle for the periodic solution. The comparison of the extracellular toxin concentration over one cycle is given in Figure 7. A comparison with Figure 4 indicates that the addition of a storage compartment has no visible influence on the concentrations. This is confirmed by Table 5, which gives the average toxin concentrations over the interdialytic phase. The reason for this phenomenon is that after a few cycles the concentration in the storage compartment reaches its maximum (compare Figure 5.

Person	large	medium	small
TAC	36.86	43.75	48.36

Table 5: Average concentration of the toxin during the interdialytic phase in case of the modified model with storage compartment ($k^{(0)}_{\mathsf{AT,S}} = 0.05$, $k_{\mathsf{rem}} = 0$).

4.3. Simulations for the model with storage compartment and degradation of toxin. The simulations in case of $k^{(0)}_{\mathsf{AT,S}} = 0.05$ and $k_{\mathrm{rem}} = 0.02$ are

presented in Figures 8 – 11. In Figure 8 we present the simulations over 10 cycles, because it takes longer till the solution approaches the periodic solution. The raggedness of some of the curves are due to non-smoothness of the right-hand side in the equations for c_{AT} and c_{S}. In addition we present in this case also the simulations for the toxin mass (Figure 10) in order to demonstrate that the toxin mass during the interdialytic phase in the large person is of course considerably larger than in the medium sized and the small person. From Table 6 we see that the average toxin concentrations are considerably smaller, if the toxin is degraded in the storage compartment. Also the differences in TAC for the three persons are much smaller, but the larger person is still a little bit better of than than medium sized person, which in turn is better of than the small person.

We also increased the degradation rate in the storage compartment and show the result of our simulations in case $k^{(0)}_{\mathsf{AT,S}} = 0.05$ and $k_{\mathrm{rem}} = 0.05$ in Figures 12 – 14. The average toxin concentrations in the extracellular compartment are presented in Table 7. We see that the concentrations are again decreased, but the large person is still better of than the other persons.

Person	large	medium	small
TAC	18.68	18.88	19.90

Table 6: Average concentration of the toxin during the interdialytic phase in case of the modified model with storage compartment and removal of the toxin from this compartment ($k^{(0)}_{\mathsf{AT,S}} = 0.05$, $k_{\mathsf{rem}} = 0.02$).

Person	large	medium	small
TAC	15.05	15.26	15.87

Table 7: Average concentration of the toxin during the interdialytic phase in case of the modified model with storage compartment and removal of the toxin from this compartment ($k^{(0)}_{\mathsf{AT,S}} = 0.05$, $k_{\mathsf{rem}} = 0.05$).

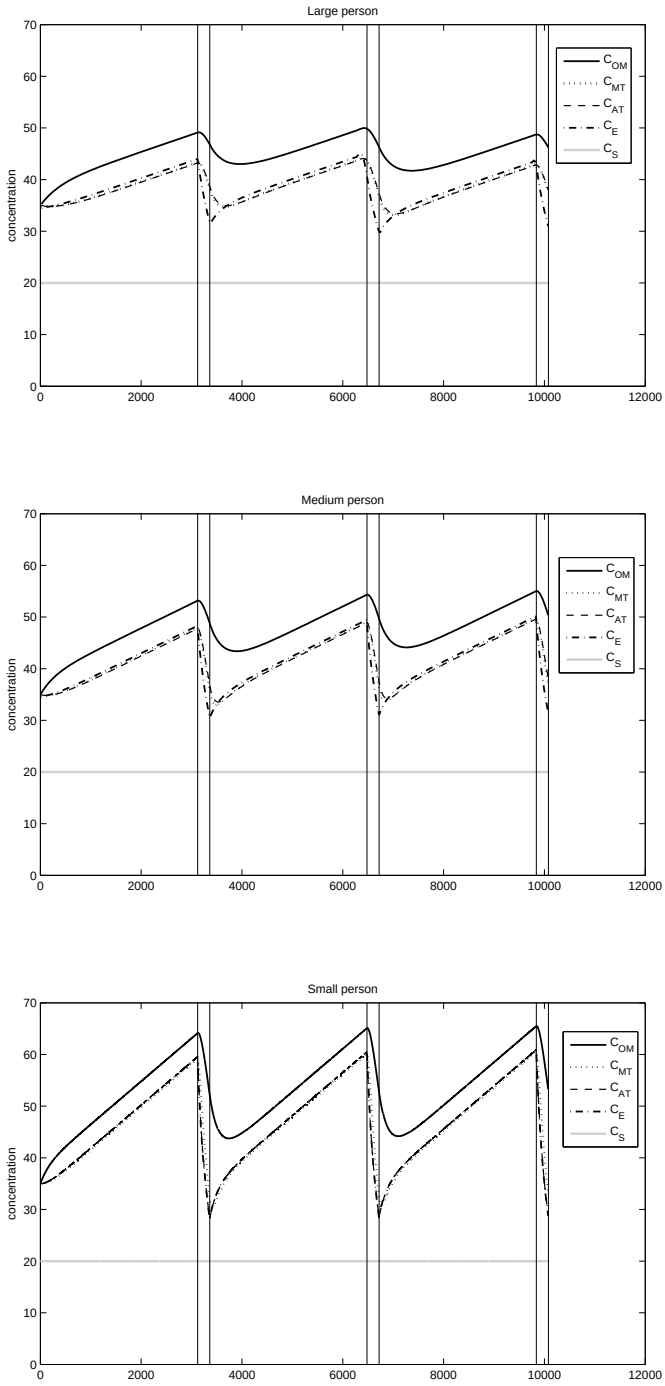

Figure 5: Simulation over three cycles for the time behavior of the toxin concentration in the compartments of the modified model with storage compartment ($k^{(0)}_{\mathsf{AT,S}} = 0.05$, $k_{\mathsf{rem}} = 0$).

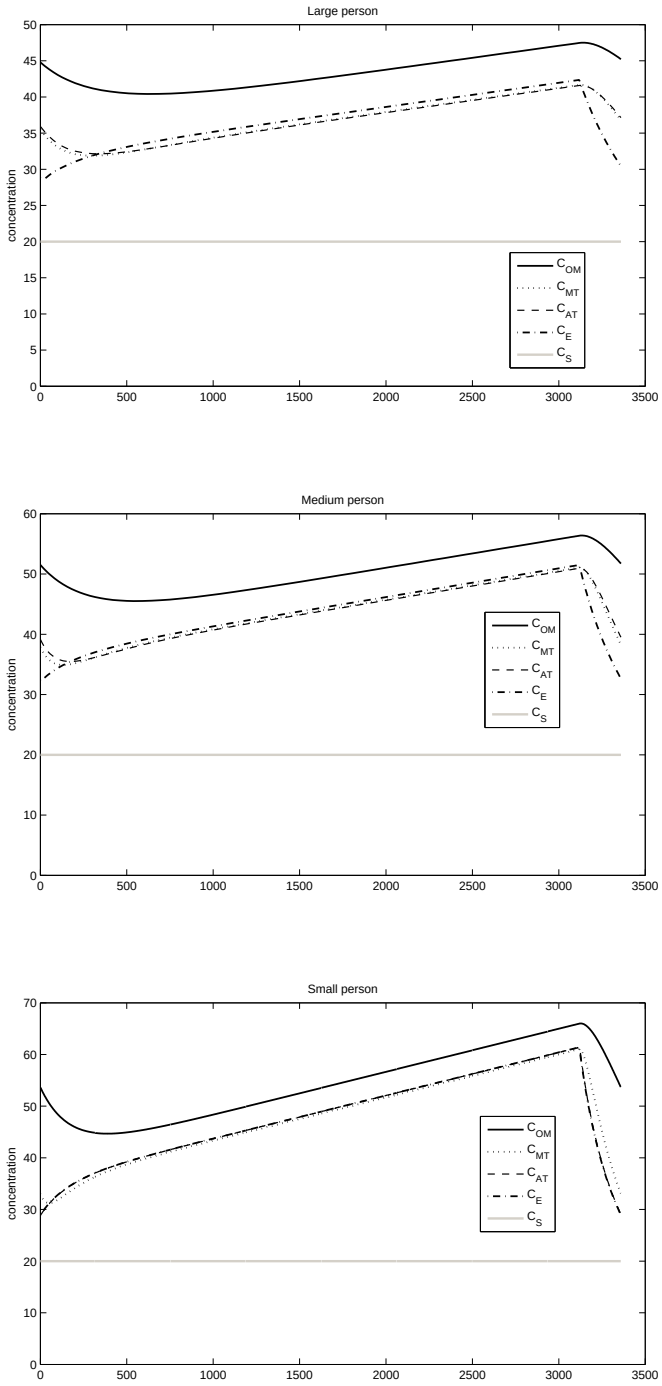

Figure 6: Simulation for the time behavior during the interdialytic period of the toxin concentration in the compartments of the modified model with storage compartment ($k^{(0)}_{\mathsf{AT,S}} = 0.05$, $k_{\mathsf{rem}} = 0$).

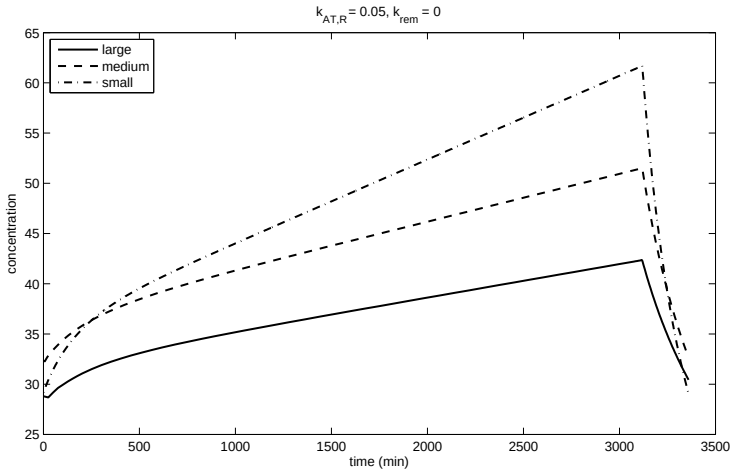

Figure 7: Comparison of the toxin concentration in the extracellular compartment for the modified model with storage compartment ($k^{(0)}_{\mathsf{AT,S}} = 0.05$, $k_{\mathsf{rem}} = 0$).

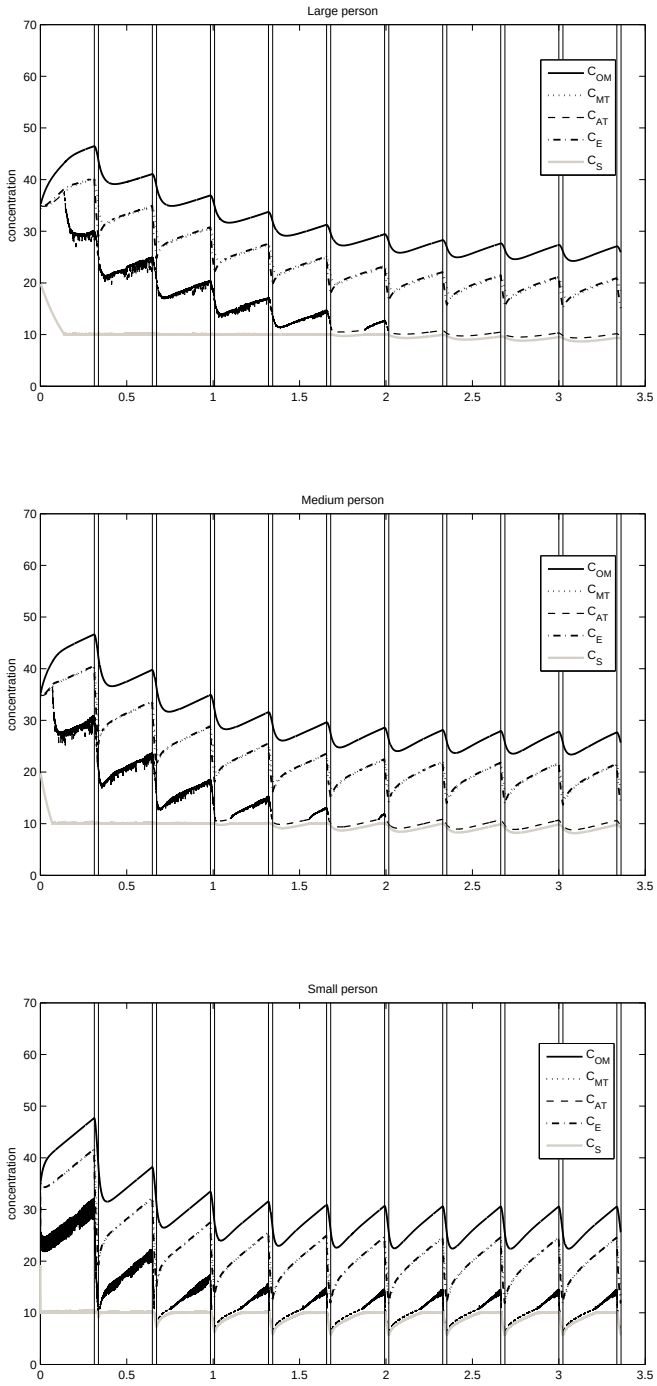

Figure 8: Simulation over three cycles for the time behavior of the toxin concentration in the compartments of the modified model with storage compartment and removal of the toxin from this compartment ($k^{(0)}_{\mathsf{AT,S}} = 0.05,\ k_{\mathsf{rem}} = 0.02$).

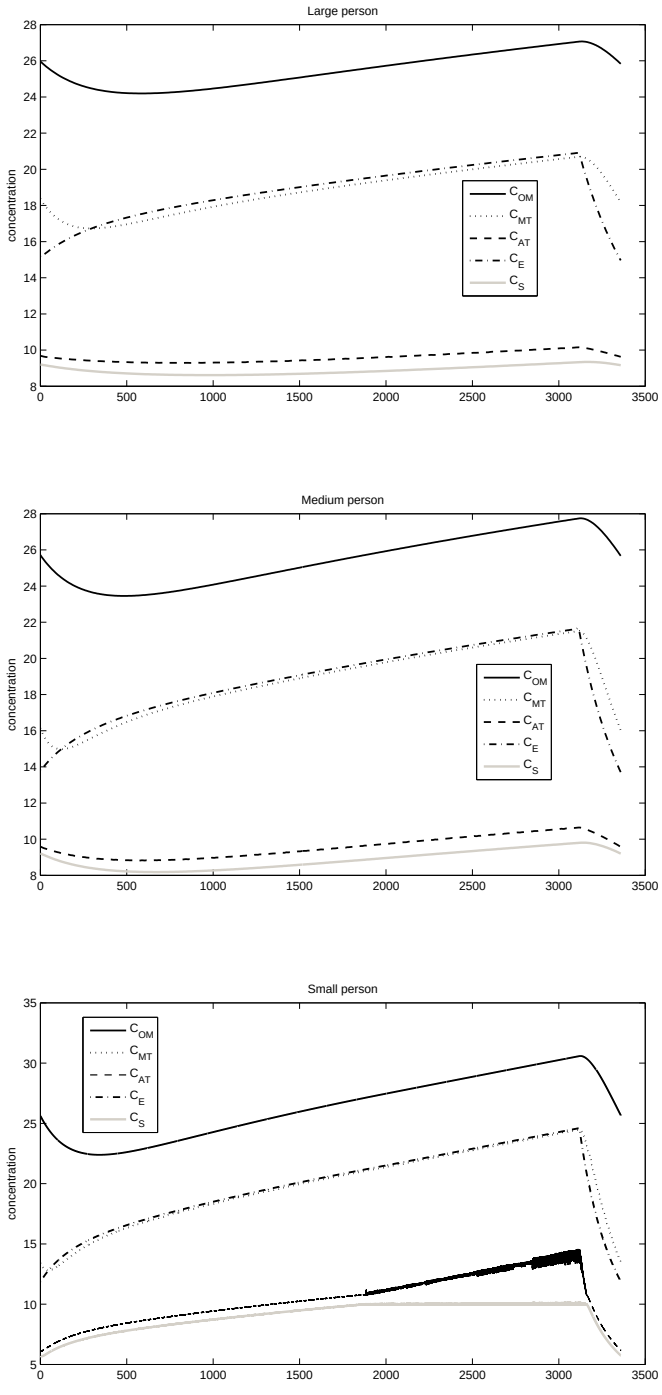

Figure 9: Simulation for the time behavior during the interdialytic period of the toxin concentration in the compartments of the modified model with storage compartment and removal of the toxin from this compartment ($k^{(0)}_{\mathsf{AT,S}} = 0.05$, $k_{\mathsf{rem}} = 0.02$).

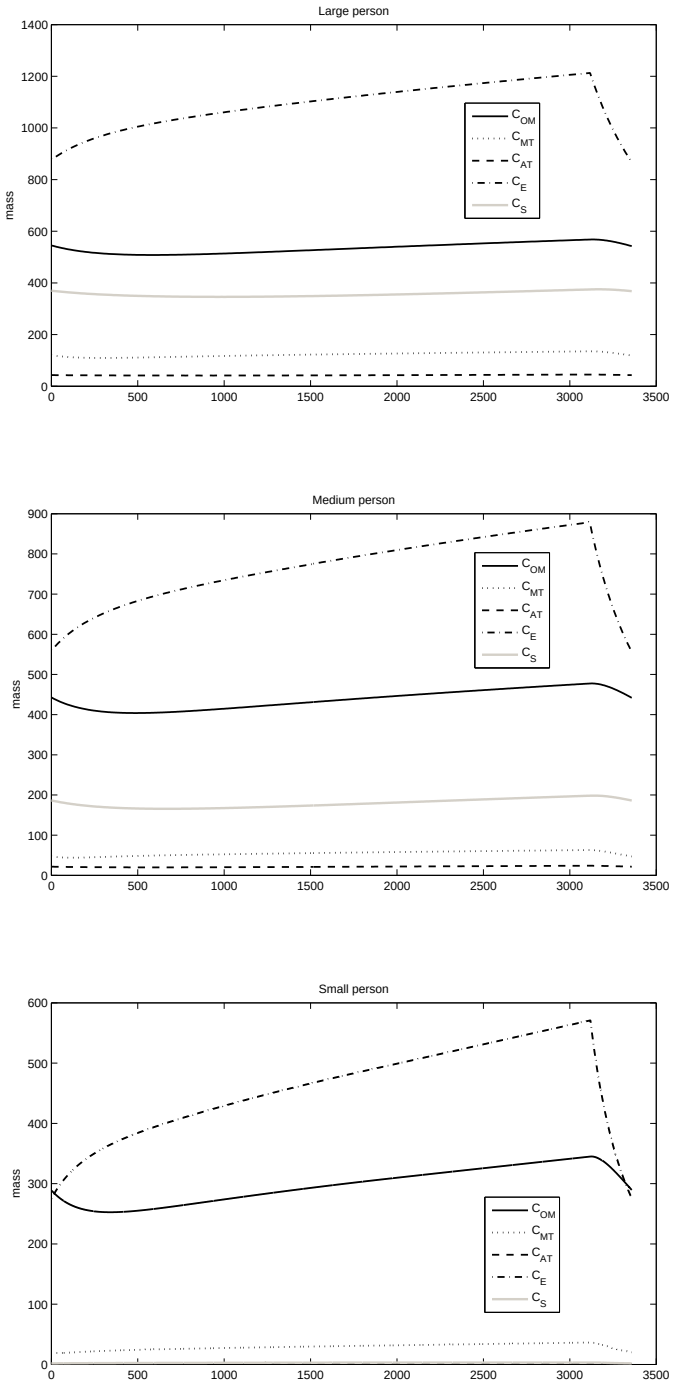

Figure 10: Simulation for the time behavior during the interdialytic period of the toxin mass in the compartments of the modified model with storage compartment and removal of the toxin from this compartment ($k^{(0)}_{\mathsf{AT,S}} = 0.05$, $k_{\mathsf{rem}} = 0.02$).

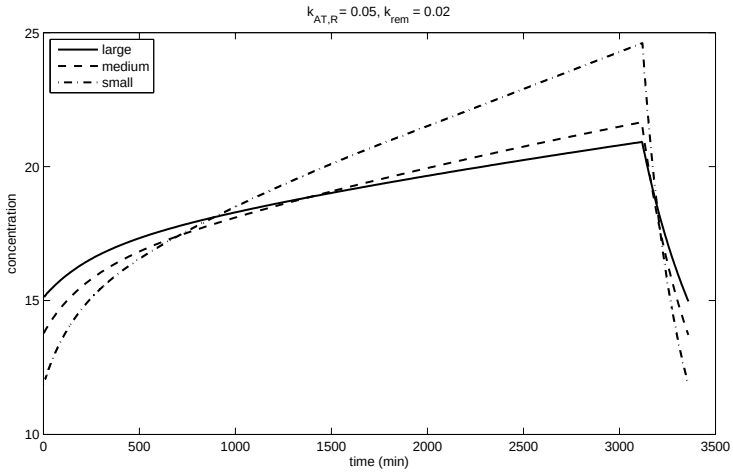

Figure 11: Comparison of the toxin concentration in the extracellular compartment for the modified model with storage compartment and removal of the toxin from this compartment ($k^{(0)}_{\mathsf{AT,S}} = 0.05$, $k_{\mathsf{rem}} = 0.02$).

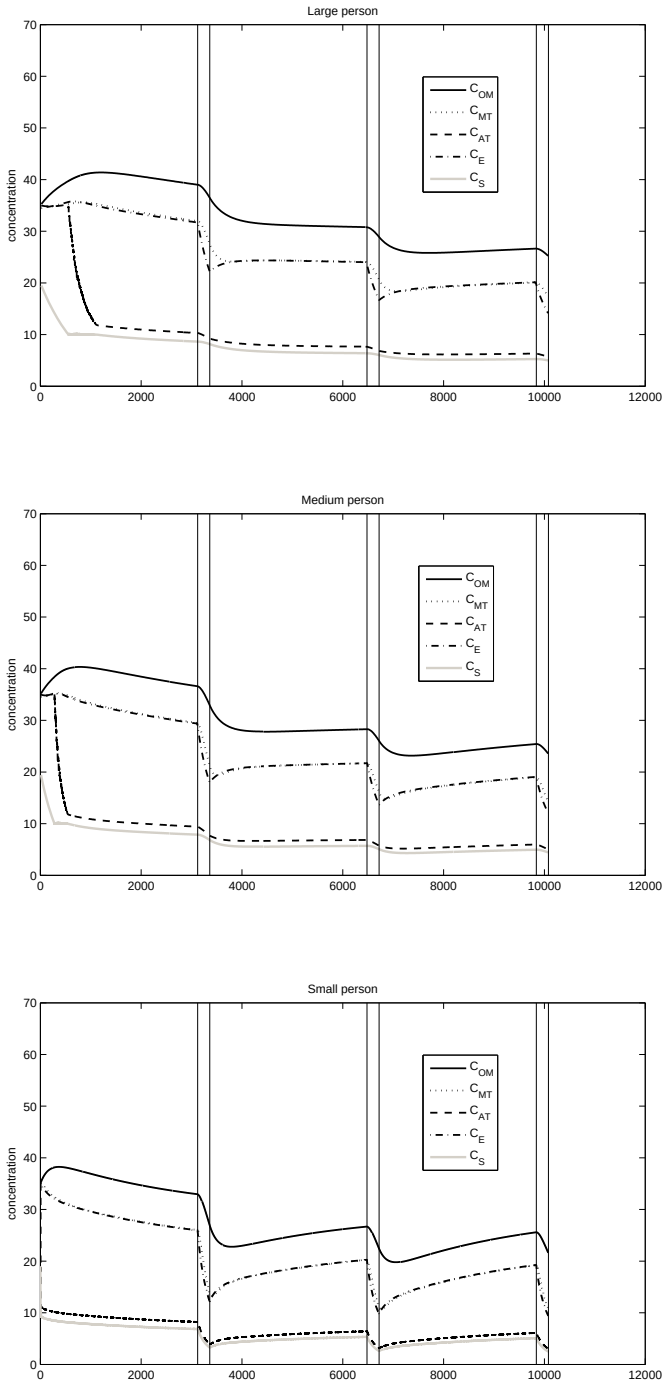

Figure 12: Simulation over three cycles for the time behavior of the toxin concentration in the compartments of the modified model with storage compartment and removal of the toxin from this compartment ($k^{(0)}_{\mathsf{AT,S}} = 0.05,\ k_{\mathsf{rem}} = 0.05$).

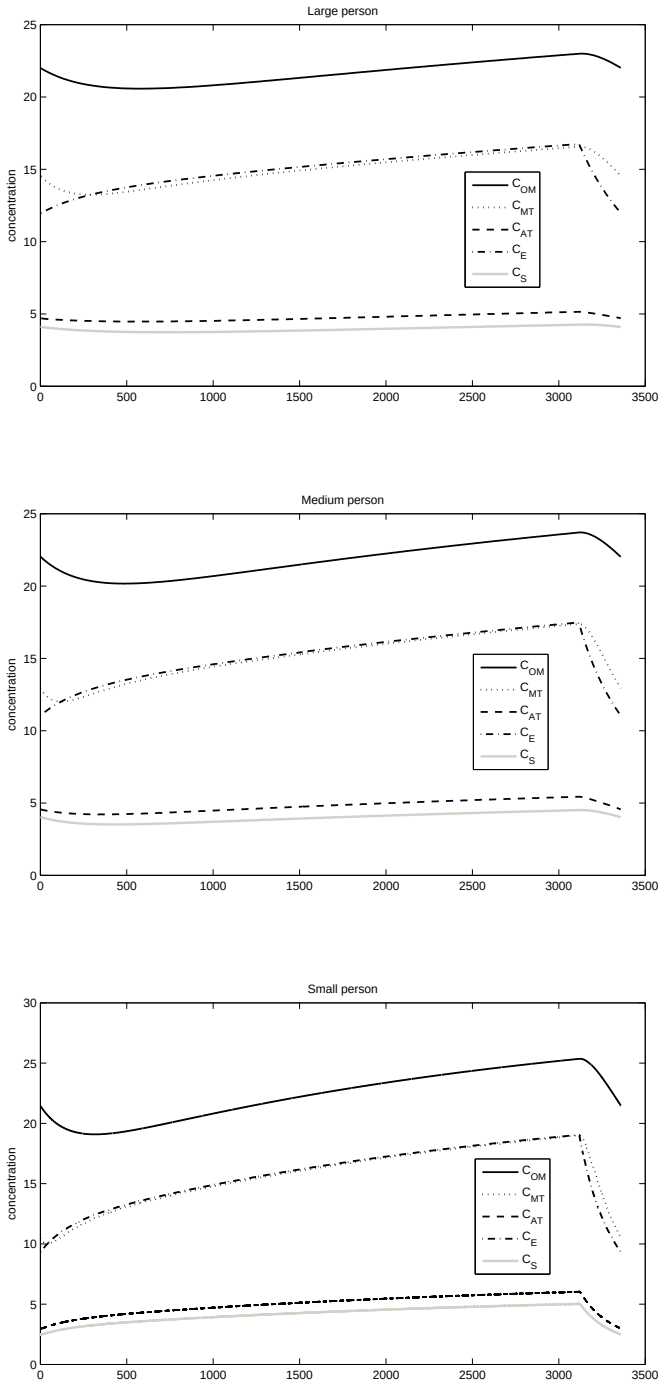

Figure 13: Simulation for the time behavior during the interdialytic period of the toxin concentration in the compartments of the modified model with storage compartment and removal of the toxin from this compartment ($k^{(0)}_{\mathsf{AT,S}} = 0.05$, $k_{\mathsf{rem}} = 0.05$).

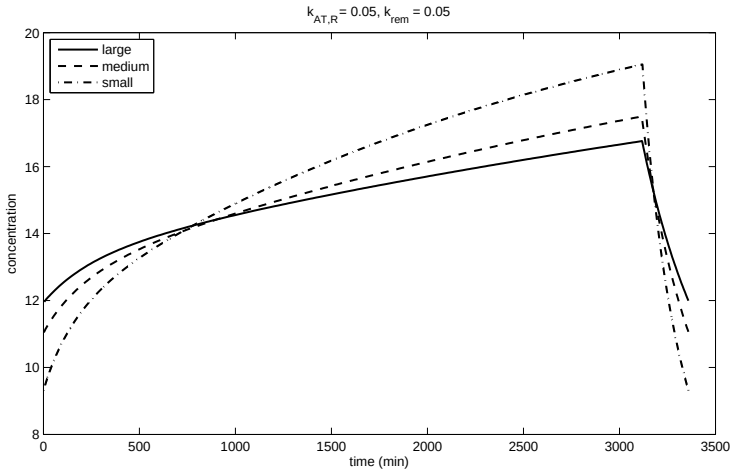

Figure 14: Comparison of the toxin concentration in the extracellular compartment for the modified model with storage compartment and removal of the toxin from this compartment ($k^{(0)}_{\mathsf{AT,S}} = 0.05$, $k_{\mathsf{rem}} = 0.05$).

4.4. Simulations for two large persons with different body composition. For the basic model we compared also the results for the large person with the results obtained for another "large" person with larger effective volume for the muscle tissue compartment and smaller effective volume for the adipose tissue compartment. Instead of $V_{\mathsf{MT}} = 6.54$, $V_{\mathsf{AT}} = 4.46$ we took $V_{\mathsf{MT}} = 12$, $V_{\mathsf{AT}} = 1$. In Figure 15 we present the concentrations during one cycle of the periodic solution. The concentrations in the extracellular compartment during one cycle for the two large persons are presented in Figure 16. We see that the toxin concentration in the extracellular compartment for the person with smaller adipose tissue compartment has a considerably large toxin concentration. This is also reflected by the TAC-values given in Table 8.

Large person		
Volumes	$V_{\mathsf{MT}} = 6.54$, $V_{\mathsf{AT}} = 4.46$	$V_{\mathsf{MT}} = 12$, $V_{\mathsf{AT}} = 1$
TAC	36.86	43.54

Table 8: Average concentration of the toxin during the interdialytic phase in case of the basic model ($k^{(0)}_{\mathsf{AT,S}} = 0$, $k_{\mathsf{rem}} = 0$) for two different choices of V_{MT} and V_{AT} for the large person.

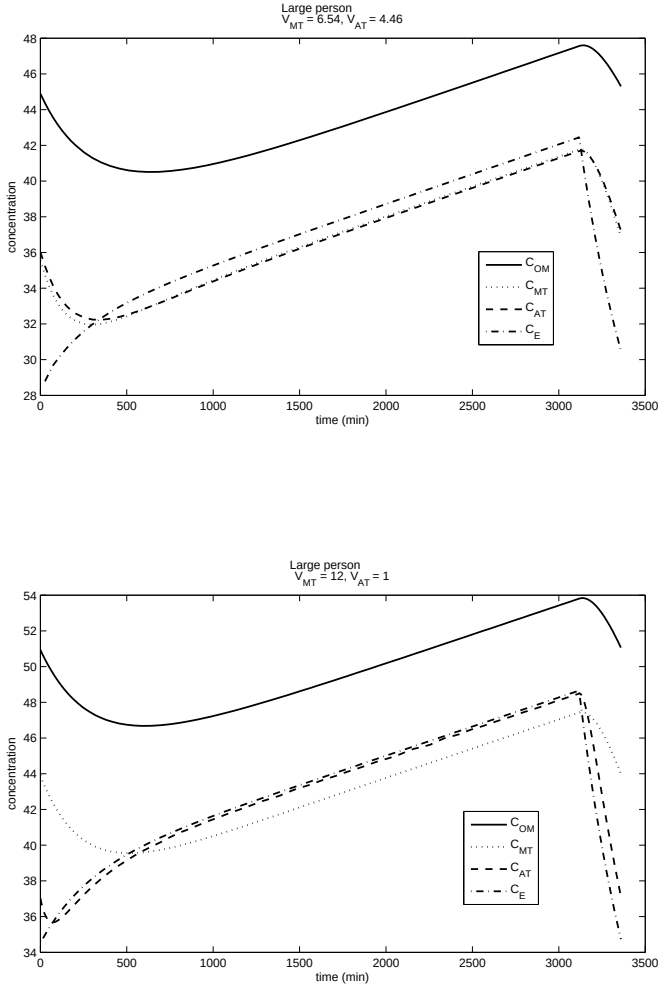

Figure 15: Simulation for the time behavior of the toxin concentration in the compartments of the basic model ($k^{(0)}_{\mathsf{AT,S}} = 0$, $k_{\mathsf{rem}} = 0$) with two different choices of the volumes V_{MT} and V_{AT}.

5. Sensitivities and generalized sensitivities

5.1. Classical sensitivities. Classical sensitivity analysis considers how model output is influenced by small changes in a parameter. It is the normalized derivative of a given model output with respect to a given parameter in the sense defined below.

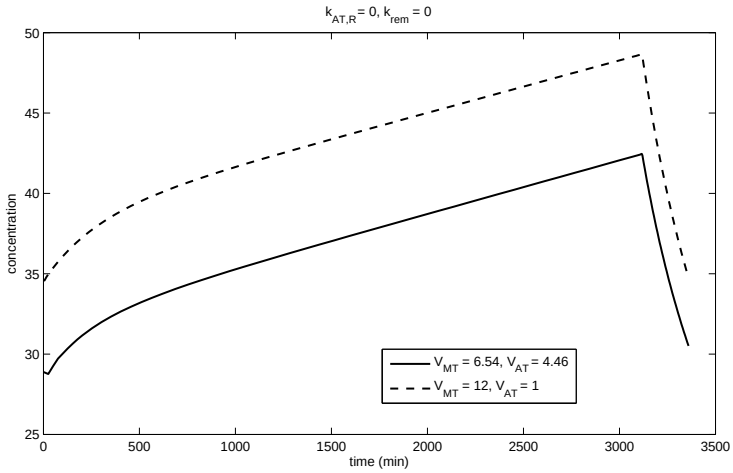

Figure 16: Comparison of the toxin concentration in the extracellular compartment for the basic model ($k^{(0)}_{\mathsf{AT,S}} = 0$, $k_{\mathsf{rem}} = 0$) for the large person with two different choices of the volumes V_{MT} and V_{AT}.

$$\lim_{\Delta p \to 0} \frac{(y_0 + \Delta y - y_0)/y_0}{(p_o + \Delta p - p_0)/p_0} = \frac{p_0}{y_0}\, y'(p_0), \tag{13}$$

where y is a single model output, p a single parameter, and y_0 and p_0 are the values around which changes are computed. Given that various outputs may have different units it is best to consider normalized derivatives as expressed above. Note that in this formulation time is fixed so that classical sensitivities are functions of time over the time interval of interest. Also note that these quantities provide local estimates of sensitivity.

We computed the sensitivities of $c_{\mathsf{E}}(t)$ with respect to the rate constants $k_{\mathsf{E,OM}}$, $k_{\mathsf{E,MT}}$, $k_{\mathsf{E,AT}}$, k_{clear} and G, i.e., we computed

$$\frac{k}{c_{\mathsf{E}}(t)}\,\frac{\partial c_{\mathsf{E}}(t)}{\partial k},$$

where k stand for one of the rate constants. The time interval considered is one cycle (i.e., $0 \le t \le 3360$) for the periodic solution. The upper two panels in Figure 17 show the sensitivities with respect to all rate constants for the small and the large person (left respectively right upper panel). We see that in both cases the sensitivities with respect to k_{clear} and G are much larger than the sensitivities with respect to $k_{\mathsf{E,OM}}$, $k_{\mathsf{E,MT}}$, $k_{\mathsf{E,AT}}$. The lower two panels show the sensitivities with respect to these three rate constants, again for the small (left panel) and the large person (right panel). Here we see that the sensitivities with respect to $k_{\mathsf{E,OM}}$ and $k_{\mathsf{E,MT}}$ are larger for the small person, whereas the sensitivity with respect to

$k_{\mathsf{E,AT}}$ is almost zero for the small person, which reflects the fact that the volume of the adipose tissue compartment for the small person is very small. From these ob-

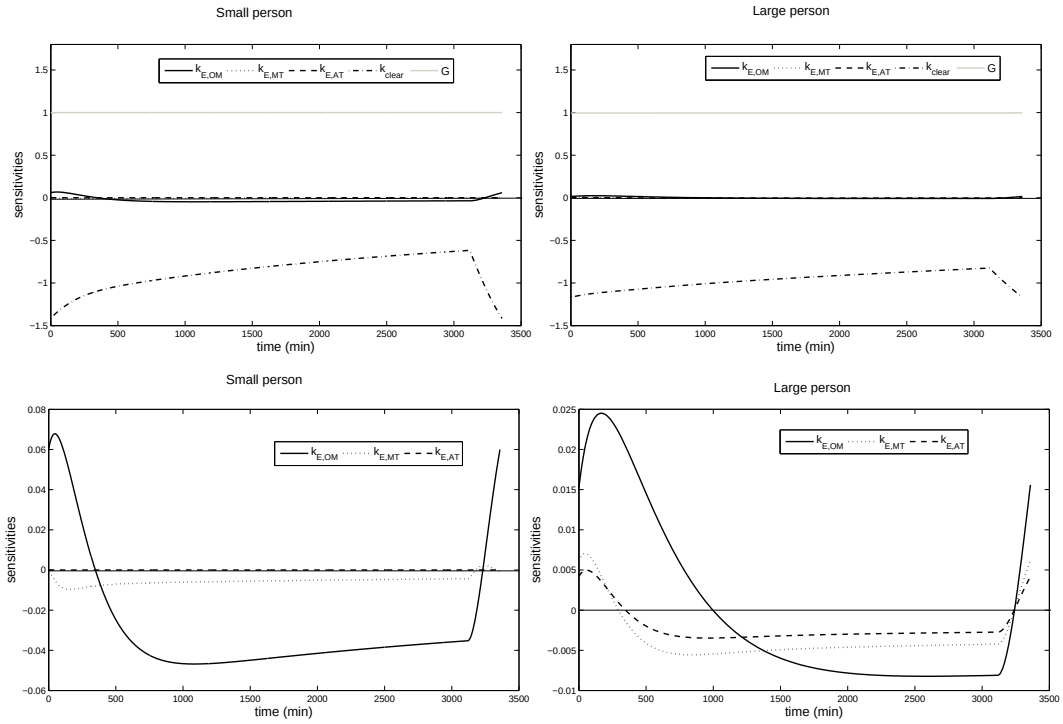

Figure 17: Sensitivities of C_{E} for the basic model ($k^{(0)}_{\mathsf{AT,S}} = 0$, $k_{\mathsf{rem}} = 0$) for the large person with respect to all parameters (upper two panels) and with respect to $k_{\mathsf{E,OM}}$, $k_{\mathsf{E,MT}}$, $k_{\mathsf{E,AT}}$ (lower two panels). The left panels are for the small person, whereas the right panels are for the large person.

servations we should expect, that identifying the rate constants $k_{\mathsf{E,OM}}$, $k_{\mathsf{E,MT}}$, $k_{\mathsf{E,AT}}$ on the basis of measurements for c_{E} should be more difficult than identifying k_{clear} (which usually is known) and G. This is confirmed by our numerical calculations (see Section **6**).

5.2. Generalized sensitivity analysis. Sensitivity functions characterize the dependence of system states and outputs on parameters. Given these relations, it is possible to examine the information content of measurements of specific state outputs of the system on certain parameters. What would be really useful to know is the sensitivity of the parameter estimates with respect to the measurements and to be able to characterize the sensitivity of the parameter estimates with respect to variations in the system parameters. For this purpose the so called generalized sensitivity functions have been introduced in [8].

Generalized sensitivity functions will be discussed for the following dynamical system model set up:

$$\begin{aligned} \dot{x}(t) &= \mathcal{F}(t, x(t), \theta), \quad x(0) = x_0(\theta), \\ \eta(t) &= h(t, x(t), \theta), \quad t \geq 0, \end{aligned}$$

where $x \in \mathbb{R}^n$ is the state vector of the system, $\eta(\cdot)$ is model output assumed to be scalar output, and $\theta \in \mathbb{R}^p$ is the vector of parameters.

The output of the above system takes the form:

$$\eta(t) = f(t;\theta), \quad t \geq 0, \tag{14}$$

The scalar output $\eta(\cdot)$ is output for which data are available, and again $\theta \in \mathbb{R}^p$ is the vector of parameters to be considered.

For the analysis which follows, the measurements for the output $\eta(\cdot)$ are assumed to be of the form

$$\xi_j = \xi_j(\theta_0) = f(t_j;\theta_0) + e_j, \quad j = 1,\dots,N, \tag{15}$$

where θ_0 is the nominal parameter vector, $0 \leq t_1 < \cdots < t_N$ are the time instance where we take the measurements and e_j, $j = 1,\dots,N$, represents the measurement noise $\mathcal{E}_j$ at t_j, which is a random variable. Here we only indicate the dependence of the ξ_j on the nominal parameter θ_0. Of course, ξ_j depends also on e_j, but this dependence will not be exploited in the developments leading to generalized sensitivity functions. It is assumed that the random variables $\mathcal{E}_j$, $j = 1,\dots,N$, are independent and identically distributed with expected values $\mathrm{E}(\mathcal{E}_j) = 0$ and variance $\sigma_j^2 = \operatorname{var}\mathcal{E}_j$, which is independent of θ_0. Consequently, the ξ_j are representations of independent and identically distributed random variables $\Xi_j = f(t_j;\theta_0) + \mathcal{E}_j$ with $\mathrm{E}(\Xi_j) = f(t_j;\theta_0)$ and $\operatorname{var}\Xi_j = \sigma_j^2$, $j = 1,\dots,N$

Given that we are interested in the impact of measurements on parameter estimation we need to consider the design of the estimation scheme which we will take to be the output-least-squares approach, where we minimize a quadratic cost functional to arrive at the parameter estimate $\hat{\theta} = \hat{\theta}(\theta_0)$. This cost functional takes the form

$$\hat{\theta} = \hat{\theta}(\theta_0) = \operatorname*{argmin}_{\tau\in\mathcal{U}} J(\tau,\xi) \tag{16}$$

in a neighborhood $\mathcal{U}$ of θ_0, where $J(\tau)$ is given as

$$J(\tau,\xi) = \sum_{j=1}^{N} \frac{1}{\sigma_j^2}\big(\xi_j - f(t_j;\tau)\big)^2 \tag{17}$$

with $\xi = \big(\xi_1,\dots,\xi_N\big)^{\mathsf{T}}$, where ξ_j is defined in (15). It is clear that, for each concrete data set ξ, the estimate $\hat{\theta}(\theta_0)$ is a representation of a random variable $\hat{\Theta}(\theta_0)$. We assume we have locally unique identifiability, i.e., for all nominal parameters in a neighborhood of θ_0 the parameter estimation problem has a unique local solution, and that the estimation procedure is unbiased, i.e., we have $\mathrm{E}(\hat{\Theta}(\theta_0)) = \theta_0$. By our assumption on unique identifiability in a neighborhood $\mathcal{U}$ of θ_0 we have

$$\nabla_\tau J(\xi(\theta),\tau)\Big|_{\tau=\hat{\theta}(\theta)} = 0, \quad \theta \in \mathcal{U}. \tag{18}$$

Given a data set $\xi(\theta)$ we want to see how the sensitivity of the parameter estimate $\hat{\theta}(\theta)$ changes as a function of $\xi^{(k)} = \big(\xi_1(\theta),\dots,\xi_k(\theta)\big)^{\mathsf{T}}$ for $k = 1,\dots,N$. This means that, for each $k = 1,\dots,N$, we are interested in $\big(\partial\hat{\theta}(\theta)/\partial\theta\big)(\theta_0)$ assuming that only the measurements in $\xi^{(k)}$ vary with θ, but the measurements $\xi_{k+1},\dots,\xi_N$ are fixed to their values for $\theta = \theta_0$. Differentiating (18) with respect to θ we obtain

$$\nabla_{\tau,\tau} J(\xi(\theta_0),\tau)\big|_{\tau=\hat{\theta}(\theta_0)} \frac{\partial\hat{\theta}}{\partial\theta}(\theta_0) + \nabla_{\xi^{(k)},\tau} J(\xi(\theta_0),\tau)\big|_{\tau=\hat{\theta}(\theta_0)} \frac{\partial\xi^{(k)}}{\partial\theta}(\theta_0) = 0. \tag{19}$$

From this equation we can compute $\partial\hat{\theta}/\partial\theta$ for all $k =, \ldots, N$, assuming that the Hessian $\nabla_{\tau,\tau} J$ is nonsingular. In doing this we take for e_j, $j = 1, \ldots, N$, and $\hat{\theta}(\theta_0)$ the expected values 0 and θ_0, respectively. We arrive at (see [1] for further details)

$$G_k(\theta_0) := \frac{\partial\hat{\theta}}{\partial\theta}(\theta_0) = \mathcal{F}(t_N, \theta_0)^{-1}\mathcal{F}(t_k, \theta_0), \quad k = 1, \ldots, N, \tag{20}$$

where we have set $\mathcal{F}(t_k, \theta_0) := \sum_{j=1}^{k}(1/\sigma_j^2)\nabla_\theta f(t_j; \theta_0)^{\mathsf{T}}\nabla_\theta f(t_j; \theta_0)$, $k = 1, \ldots, N$. The matrix $\mathcal{F}(t_k, \theta_0)$ is nothing else than the Fisher information matrix for our parameter estimation problem. Under additional assumptions, the quantity $G_k(\theta_0)$ can be considered as an approximation of the expected value of the Jacobian $(\partial\hat{\theta}_0/\partial\theta)(\theta_0)$ for the case when only the first k measurements are assumed to vary with θ.

The *generalized sensitivity functions* are given by the main diagonal elements of G_k:

$$g_i(t_k, \theta_0) := \big(G_k(\theta_0)\big)_{i,i}, \quad i = 1, \ldots, p, \ k = 1, \ldots, N.$$

The behavior of g_i as a function of the measurement times allows conclusions on the information content of measurements on the parameter θ_i. Two main points are mentioned:

- If information on parameters in the measurements is not correlated then the sensitivity functions g_i are almost monotonically increasing from $g_i(t_1)$ to $g_i(t_N) = 1$. Otherwise, the g_i's show oscillatory behavior.
- Measurements in a time range where g_i is rapidly changing contain more information than those where g_i is slowly varying. This analysis indicates that in order to improve the parameter estimates one should increase the number of measurements on those time regions where the generalized sensitivities are varying more than in other regions.

For a fuller discussion of these features, see [1] and [8].

5.3. Generalized sensitivities examined. From the generalized sensitivity functions computed for each rate constant individually (see Figure 18 for the case where measurements are only taken during the interdialytic phase and Figure 19 concerning the dialytic phase) we see that the distribution of the information content of the corresponding measurements on the parameters $k_{\mathsf{E,MT}}$, $k_{\mathsf{E,AT}}$ is almost identical. The same is true for the pair of rates k_{clear}, G. For the dialytic phase we see an almost identical distribution for the triple $k_{\mathsf{E,OM}}$, $k_{\mathsf{E,MT}}$, $k_{\mathsf{E,AT}}$. These observations are also shown by the generalized sensitivity functions for the rates when they are computed simultaneously for all five rates (see Figures 20 and 21). We see that the oscillations of the generalized sensitivity functions for $k_{\mathsf{E,MT}}$, $k_{\mathsf{E,AT}}$ are strongly correlated. The same is true for the rates k_{clear}, G. The oscillations of the generalized sensitivity function for $k_{\mathsf{E,OM}}$ are less correlated to those of the generalized sensitivity function for $k_{\mathsf{E,MT}}$, $k_{\mathsf{E,AT}}$ during the interdialytic phase compared to the dialytic phase. If we compute the generalized sensitivity functions for the pair k, G, where k stands for each one of the rates $k_{\mathsf{E,OM}}$, $k_{\mathsf{E,MT}}$, $k_{\mathsf{E,AT}}$, then the generalized sensitivity functions for k and G are almost identical to those shown in Figure 18 and Figure 19, respectively. The same observation can be made when we take k_{clear} instead of G (see Figure 22). From these observations together with the information obtained from the sensitivity functions (as presented in the previous

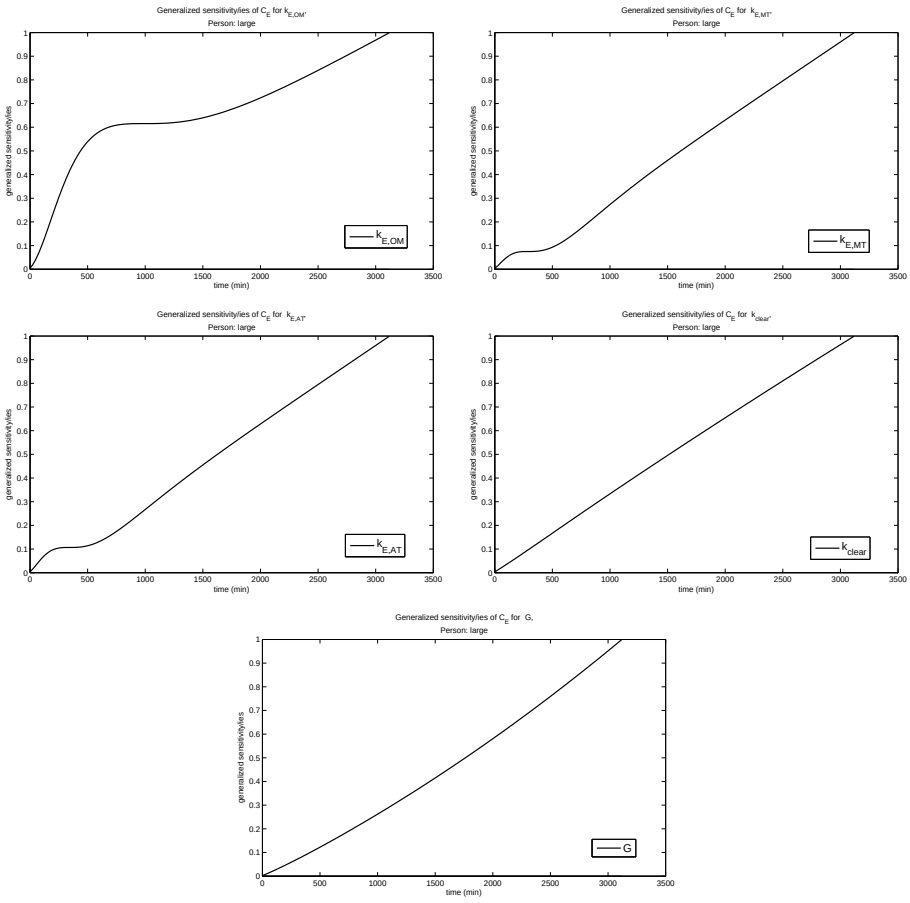

Figure 18: Generalized sensitivities of C_{E} with respect to the rate constants for the basic model ($k^{(0)}_{\mathsf{AT,S}} = 0$, $k_{\mathsf{rem}} = 0$) for the large person. Time interval is the interdialytic phase when the solution already is periodic.

subsection) we should expect the following behavior of the numerical algorithms used for parameter identification:

- Despite the fact that the information of measurements on the parameters k_{clear} and G is strongly correlated the algorithms should behave reasonably well, because of the high sensitivity of the measured output with respect to these parameters.
- For the parameters $k_{\mathsf{E,OM}}$, $k_{\mathsf{E,MT}}$, $k_{\mathsf{E,AT}}$ we should expect difficulties in view of the low sensitivity of the measured output with respect to these parameters.
- If we want to identify one of the parameters $k_{\mathsf{E,OM}}$, $k_{\mathsf{E,MT}}$, $k_{\mathsf{E,AT}}$ together with G or k_{clear} then the results should be good concerning G or k_{clear}, but also better for the other parameter in comparison to the previous item.

These observations are confirmed by the numerical computations presented in Section **6**.

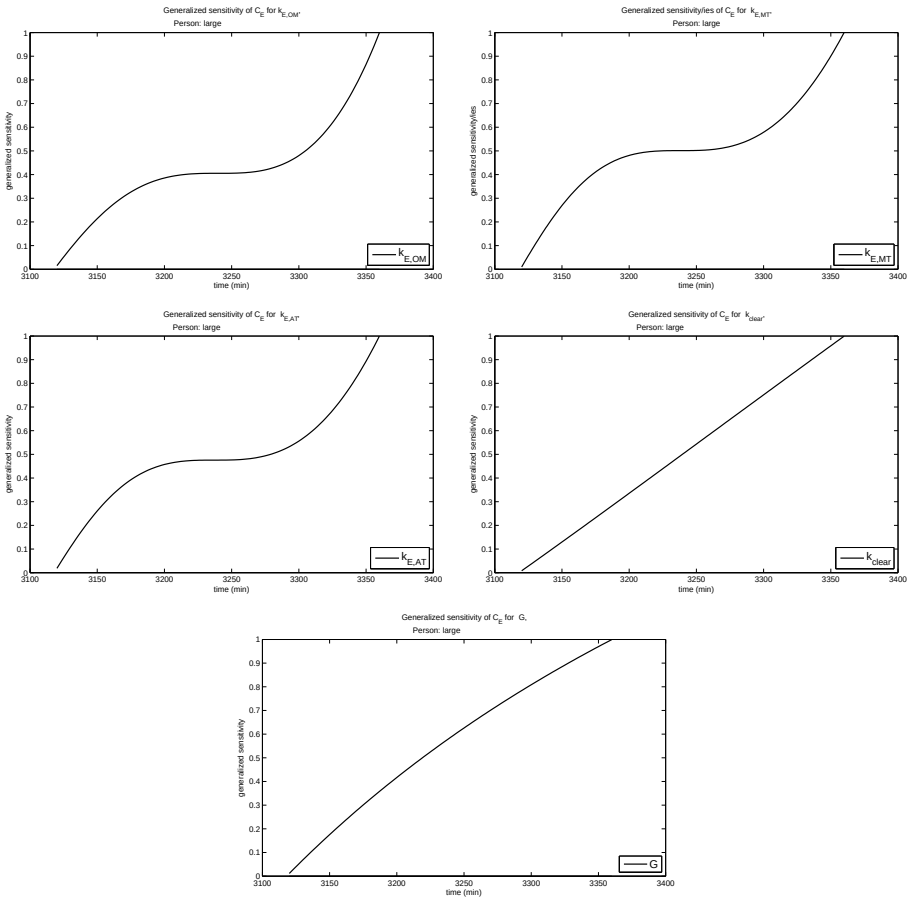

Figure 19: Generalized sensitivity of C_{E} with respect to the rate constants for the basic model ($k^{(0)}_{\mathsf{AT,S}} = 0$, $k_{\mathsf{rem}} = 0$) for the large person. Time interval is the dialytic phase when the solution already is periodic.

6. Parameter identification

The vector of parameters of the system is $\theta = \mathrm{col}\big(k_{\mathsf{E,OM}}, k_{\mathsf{E,MT}}, k_{\mathsf{E,AT}}, k_{\mathrm{clear}}, G\big) \in \mathbb{R}^5$. The toxin concentration in the extra-cellular compartment is a natural candidate for the measurable output y of the system,

$$y(t,\theta) = c_{\mathsf{E}}(t,\theta), \quad t \geq 0.$$

We assume that measurements are available at time instants $0 \leq t_1 < \cdots < t_N$ and that these measurements are given by

$$\xi_j = y(t_j,\theta_0) + \epsilon_j, \quad j = 1,\ldots,N,$$

where θ_0 is the 'true' or nominal parameter vector and ϵ_j is a representation of the measurement noise $\mathcal{E}_j$ at t_j with $\mathrm{E}(\mathcal{E}_j) = 0$ and $\mathrm{var}\,\mathcal{E}_j = \sigma_j^2$.

For our numerical experiments we took

$$\theta_0 = \mathrm{col}(0.045, 0.03177, 0.0193, 0.1, 0, 3)$$

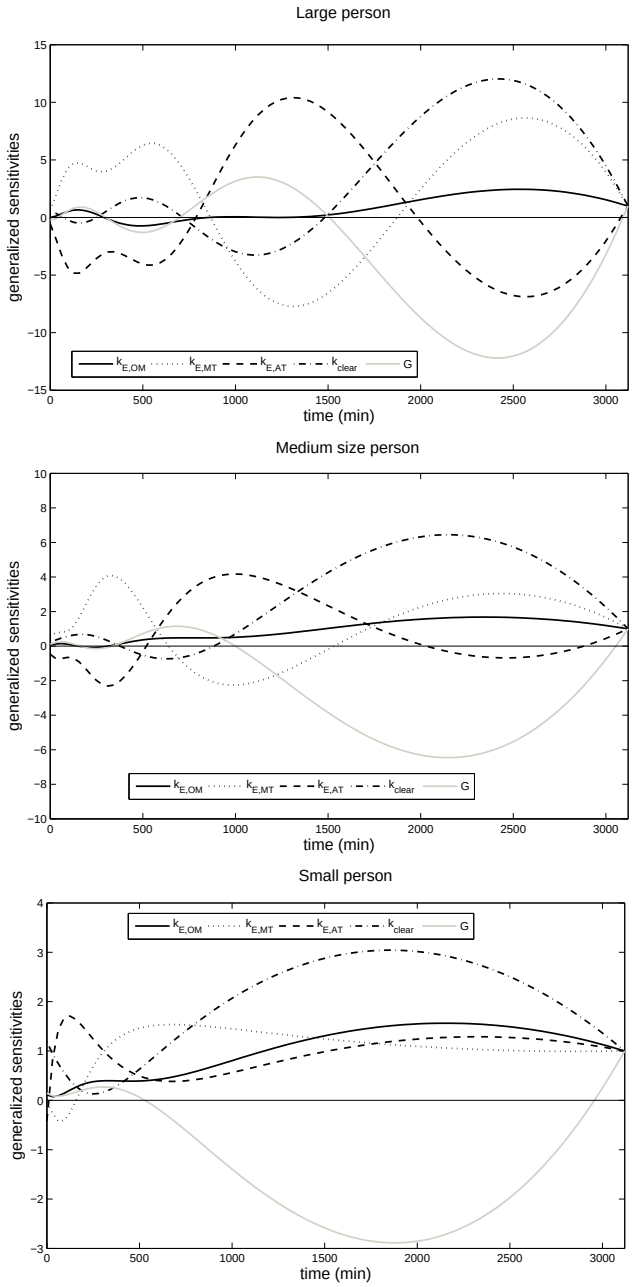

Figure 20: Generalized sensitivities of C_{E} simultaneously with respect to all rate constants for the basic model ($k^{(0)}_{\mathsf{AT,S}} = 0$, $k_{\mathsf{rem}} = 0$) for the large, the medium and the small person. Time interval is the interdialytic phase when the solution already is periodic.

and assumed that the variance σ_j^2 is constant, $\sigma_j = \sigma$, $j = 1, \ldots, N$. The parameter estimate $\hat{\theta}_0$ is obtained as a minimization of an error functional J,

$$\hat{\theta}_0 = \underset{\theta}{\operatorname{argmin}}\, J(\xi, \theta),$$

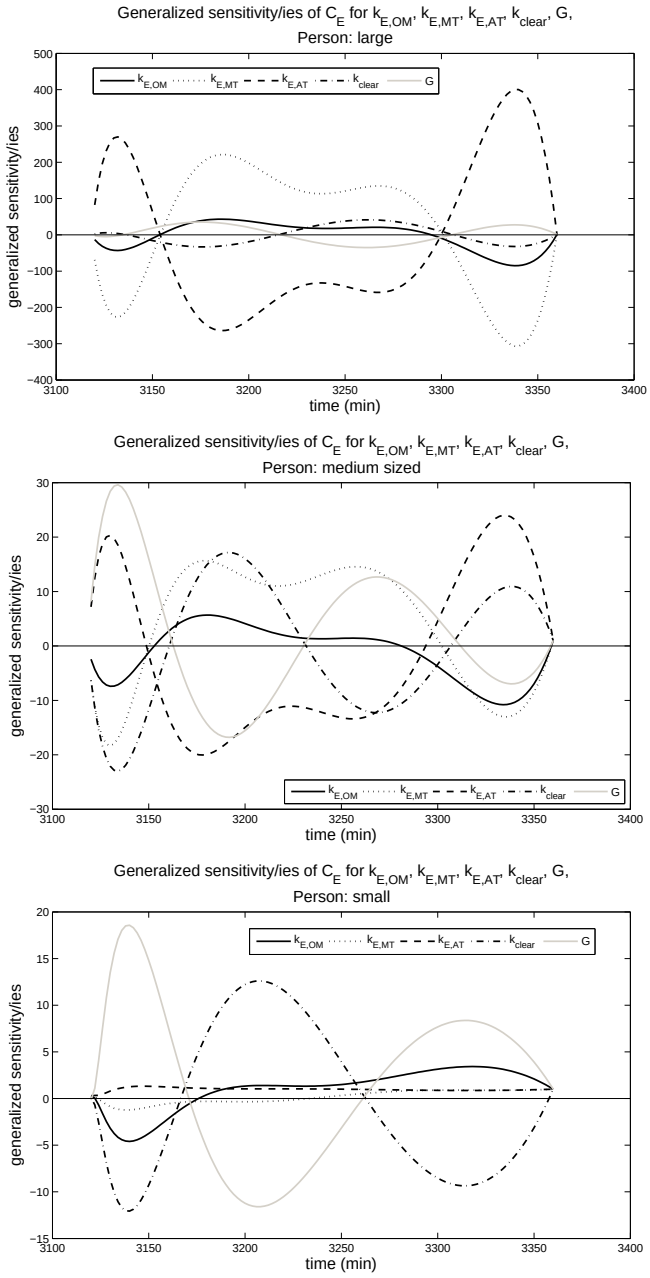

Figure 21: Generalized sensitivities of C_{E} simultaneously with respect to all rate constants for the basic model ($k^{(0)}_{\mathsf{AT,S}} = 0$, $k_{\mathsf{rem}} = 0$) for the large, the medium and the small person. Time interval is the dialytic phase when the solution already is periodic.

where $\xi = \mathrm{col}(\xi_1, \dots \xi_N)$. We considered two cases:

$$J = J_{\mathrm{qu}}(\xi, \theta) := \sum_{j=1}^{N} (\xi_j - y(t_j, \theta))^2,$$

$$J = J_{\mathrm{abs}}(\xi, \theta) := \sum_{j=1}^{N} \big|\xi_j - y(t_j, \theta)\big|.$$

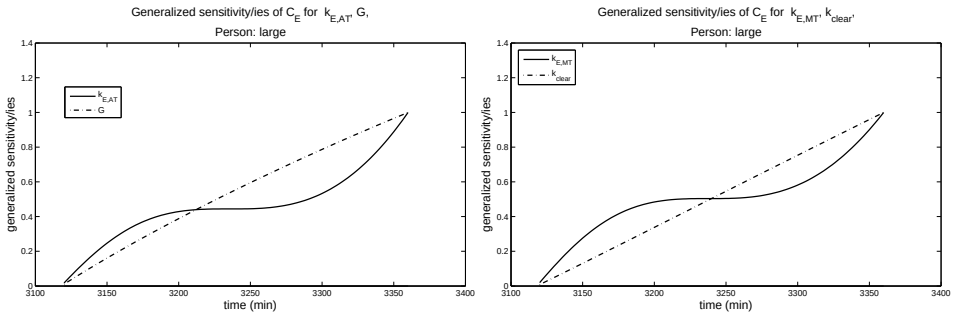

Figure 22: Generalized sensitivities of C_{E} with respect to $k_{\mathsf{E,AT}}$, G (left panel) and with respect to $k_{\mathsf{E,MT}}$, k_{clear} (right panel) during the dialytic phase.

Two optimization algorithms were used, the MatLab-implementation fminsearch of the Nelder-Mead algorithm (see [7]) and solvopt, an implementation of Shor's r-algorithm (see [4] and [6]). Both algorithms can handle non-smooth functions. For the error functional J_{qu} solvopt was used with gradient information and for J_{abs} without gradient information. In most cases the performance of the two algorithms is comparable. However, in cases where the measured output is not very sensitive with respect to the parameters to be identified solvopt is somewhat more accurate, whereas fminsearch is considerably faster.

In Table 9 we present the results for the parameters k_{clear} and G. Starting values for the algorithms where always $k_{\mathrm{clear}} = 0.5$, $G = 0.8$. We generated 6 respectively 21 uniformly distributed measurements during the dialytic phase by computing the solution of our model corresponding to the nominal parameter vector θ_0 at the measurement times and adding normally distributed noise with expected value zero and variance $\sigma = 1$. In Figure 23 we present the graphs for two of these cases. In Figure 24 we present the results for the same parameters but with 21 uniformly measurements distributed measurements during the dialytic phase.

Algorithm	Error functional	(k_{clear}, G)
6 measurements during the dialytic phase		
solvopt	J_{qu}	(0.0911 0.2739)
solvopt	J_{abs}	(0.0872 0.2636)
fminsearch	J_{qu}	(0.1040 0.3113)
fminsearch	J_{abs}	(0.0904 0.2780)
21 measurements during the dialytic phase		
solvopt	J_{qu}	(0.0974 0.2960)
fminsearch	J_{qu}	(0.0951 0.2891)

Table 9: Identification of k_{clear} and G using 6 respectively 21 measurements during the dialytic phase.

In order to check the conclusions we made in Subsection **5.3** we tried to identify the rates $k_{\mathsf{E,MT}}$ and $k_{\mathsf{E,AT}}$. As starting values for the optimization algorithms we did choose

$$k_{\mathsf{E},MT} = 0.15, \quad k_{\mathsf{E,AT}} = 0.1\,.$$

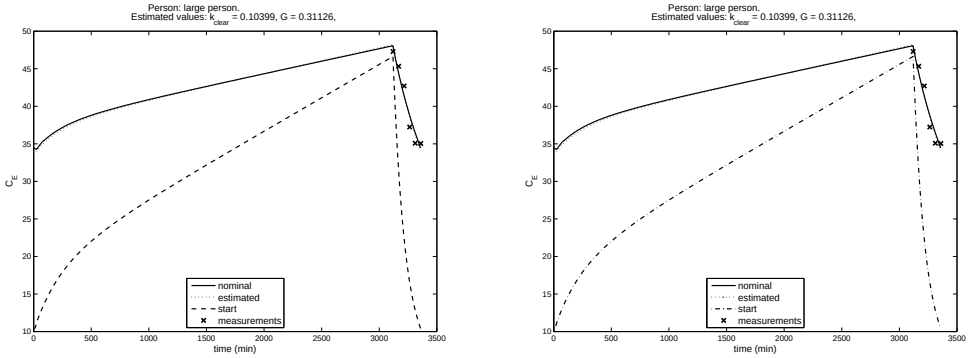

Figure 23: Estimates for k_{clear} and G using 6 measurements during the dialytic phase using solvopt (left panel) respectively fminsearch (right panel) for the error functional for J_{qu}.

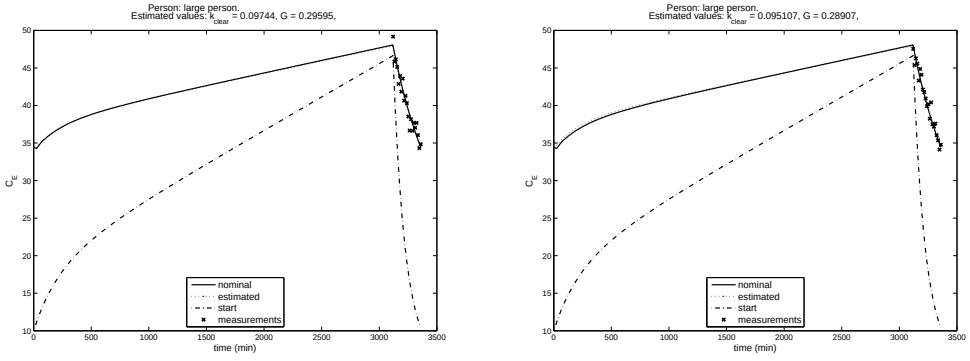

Figure 24: Estimates for k_{clear} and G using 21 measurements during the dialytic phase using solvopt (left panel) respectively fminsearch (right panel) for the error functional for J_{qu}.

The estimates were again done with 6 respectively 21 measurements uniformly distributed during the dialytic phase and computed as in the previous case. Some of our findings are shown in Table 10. If we compare the estimates with the nominal

Algorithm	Error functional	$(k_{\mathsf{E},MT}, k_{\mathsf{E},AT})$
6 measurements during the dialytic phase		
solvopt	J_{qu}	$(0.0773 \quad 0.0556)$
fminsearch	J_{qu}	$(0.1616 \quad 0.0954)$
21 measurements during the dialytic phase		
solvopt	J_{qu}	$(0.2440 \quad 0.1952)$
fminsearch	J_{qu}	$(0.1616 \quad 0.0954)$

Table 10: Identification of $k_{\mathsf{E,MT}}$ and $k_{\mathsf{E,AT}}$ using 6 respectively 21 measurements during the dialytic phase.

values $k_{\mathsf{E,MT}} = 0.0318$ and $k_{\mathsf{E,AT}} = 0.0193$ we see that the conclusions of Subsection **5.3** are correct. In Figure 25 we depict the results obtained with solvopt.

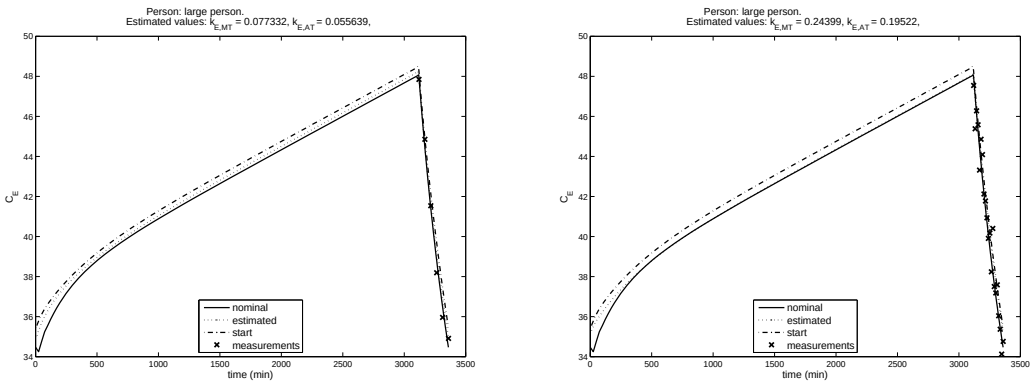

Figure 25: Estimates for $k_{\mathsf{E,MT}}$ and $k_{\mathsf{E,AT}}$ using solvopt with 6 (left panel) respectively 21 remeasurements (right panel) during the dialytic phase for the error functional for J_{qu}.

Finally, we identified $k_{\mathsf{E,AT}}$ and G, again using 6 respectively 21 uniformly distributed measurements during the dialytic phase, which were computed as in the previous cases. We used the starting values

$$k_{\mathsf{E,AT}} = 0.1, \quad G = 0.8\,.$$

The results are given in Table 11, whereas Figure 26 shows the graphs corresponding to the estimates obtained with solvopt.

Algorithm	Error functional	$(k_{\mathsf{E},AT}, G)$
6 measurements during the dialytic phase		
solvopt	J_{qu}	$(0.0300 \quad 0.2944)$
fminsearch	J_{qu}	$(0.1269 \quad 0.2910)$
21 measurements during the dialytic phase		
solvopt	J_{qu}	$(0.6551 \quad 0.2949)$
fminsearch	J_{qu}	$(0.1292 \quad 0.2929)$

Table 11: Identification of $k_{\mathsf{E,AT}}$ and G using 6 respectively 21 measurements during the dialytic phase.

7. Final observations

Based on the model and model simulations presented here we can give the following observations.

- For this model higher levels of extracellular uremic toxin in the interdialytic phase will appear in patients with lower BMI under certain conditions on the compartment exchange rates.

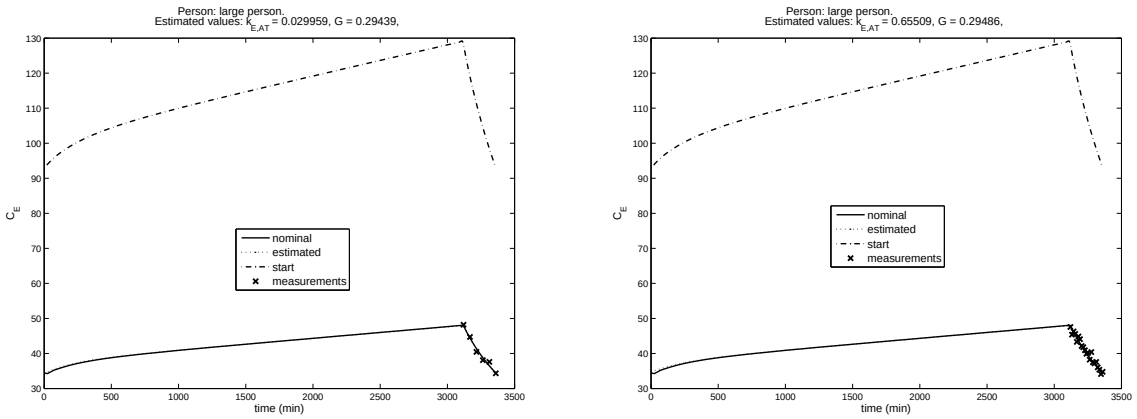

Figure 26: Estimates for $k_{\mathsf{E,AT}}$ and G using solvopt with 6 (left panel) respectively 21 measurements (right panel) during the dialytic phase for the error functional for J_{qu}.

- Hence the model simulations indicate that the mechanisms hypothesized in [3] could account for the survival advantage of high BMI dialysis patients.
- These mechanisms depend on the assumptions that the proportion of organ mass is higher in low BMI patients and that adipose tissue (higher in high BMI patients) acts as a buffer for uremic toxins. Taken together these factors would imply a higher extracellular toxin concentration in lower BMI patients. Model simulations indicate that these factors could produce such higher toxin concentrations in low BMI patients.
- Generalized sensitivity analysis indicates that parameter estimation for this model is not improved by data during the interdialytic phase which is an advantage given that it would be difficult to have dialysis patients return to the hospital for measurements in between dialysis sessions.
- The classical and generalized sensitivity analysis indicates that several parameter combinations can be identified using only data from the intradialytic phase.

Acknowledgements

This research was partially funded by Austrian Research Funds Project 18778-N13.

References

[1] J. J. Batzel and F. Kappel and H. T. Tran and D. Schneditz, *Cardiovascular and Respiratory Systems: Modeling, Analysis, and Control*, Siam, Philadelphia (2006).

[2] S. Beddhu and L. M. Pappas and N. Ramkumar and M. Samore, *Effects of Body Size and Body Composition on Survival in Hemodialysis Patients*, J Am Soc Nephrol **14** (2003), 2366 – 2372.

[3] D. Cronin-Fine, F. Gotch, N. Levin, P. Kotanko, and M. Lysaght, *A mathematical model comparing solute kinetics in low- and high-BMI hemodialysis patients*, Internatl. J. Artificial Organs **30**(11) (2007), 1000 – 1007.

[4] F. Kappel and A. V. Kuntsevich, *An implementation of Shor's r-algorithm*, Computatuional Optimization and Applications **15** (2000), 193 – 205.

[5] K. Kalantar-Zadeh and K. C. Abbott and A. K. Salahudeen and R. D. Kilpatrick and T. B. Horwich, *Survival advantages of obesity in dialysis patients*, Am J Clin Nutrition **81** (2005), 543 – 554.

[6] A. V. Kuntsevich and F. Kappel, http://www.kfunigraz.ac.at/imawww/kuntsevich/solvopt/.

[7] J. A. Nelder and R. Mead, *A simplex method for function minimization*, Computer Journal, (1965), 308 – 313.

[8] K. Thomaseth and C. Cobelli, *Generalized sensitivity functions in physiological system identification*, Ann Biomedical Eng **27** (1999), 607 – 616.

[9] F. K Port and V. B. Ashby and R. K. Dhingra and E.C. Roys and R. A. Wolfe, *Dialysis Dose and Body Mass Index Are Strongly Associated with Survival in Hemodialysis Patients*, J Am Soc Nephrol **13** (2002), 1061 – 1066.

[10] R. A. Wolfe and V. B. Ashby and J. T. Daugirdas and L. Y. Agodoa ad C. A. Jones and F. K. Port, *Body Size, Dose of Hemodialysis, and Mortality*, Am J Kidney Dis **35** (2000), 80 – 88.

F. Kappel: Institute for Mathematics and Scientific Computing, University of Graz, Heinrichstrasse 36, A 8010 Graz, Austria.

E-mail address: franz.kappel@uni-graz.at